

Coronavirus TGEV Evades the Type I Interferon Response through IRE1 α -Mediated Manipulation of the miR-30a-5p/SOCS1/3 Axis

Yanlong Ma^{#,1}, Changlin Wang^{#,2}, Mei Xue¹, Fang Fu¹, Xin Zhang¹, Liang Li¹,
Lingdan Yin¹, Wanhai Xu², Li Feng^{1,*}, Pinghuang Liu^{1,*}

1. State Key Laboratory of Veterinary Biotechnology, Harbin Veterinary
Research Institute, Chinese Academy of Agricultural Sciences, Harbin, China,
150069; 2. Department of Urology, the Fourth Affiliated Hospital of Harbin
Medical University, Harbin, Heilongjiang Province, China, 150001

Running title: TGEV escapes IFN-I via the miR-30a-5p/SOCS pathway

*Corresponding authors:

Pinghuang Liu, Ph.D., E-mail: liupinghuang@caas.cn

Li Feng, Ph.D., E-mail: fengli@caas.cn

[#], these authors contributed equally to this work

Abstract word count: 187

Text word count: 6229

Abstract

In host innate immunity, type I interferons (IFN-I) are major antiviral molecules, and coronaviruses have evolved diverse strategies to counter the IFN-I response during infection. Transmissible gastroenteritis virus (TGEV), a member of the alphacoronavirus family, induces endoplasmic reticulum (ER) stress and significant IFN-I production after infection. However, how TGEV evades the IFN-I antiviral response despite the marked induction of endogenous IFN-I has remained unclear. IRE1 α , a highly conserved ER stress sensor with both kinase and RNase activities, is involved in the IFN response. In this study, IRE1 α facilitated TGEV replication via downmodulating the host miR-30a-5p abundance. miR-30a-5p normally enhances IFN-I antiviral activity by directly targeting the negative regulators of JAK-STAT, SOCS1 and SOCS3. Furthermore, TGEV infection increased SOCS1 and SOCS3 expression, which dampened IFN-I antiviral response and facilitated TGEV replication. Importantly, compared with mock infection, TGEV infection *in vivo* resulted in decreased miR-30a-5p levels and significantly elevated SOCS1 and SOCS3 expression in piglet ileum. Taken together, our data reveal a new strategy used by TGEV to escape the IFN-I response by engaging the IRE1 α -miR-30a-5p-SOCS1/3 axis, thus improving our understanding of how TGEV escapes host innate immune defenses.

Key words: Transmissible gastroenteritis virus (TGEV), IRE1 α , miR-30a-5p, SOCS, Type I interferon

46 **Importance:** Type I interferons (IFN-I) play essential roles in restricting viral
47 infections. Coronavirus infection induces ER stress and the interferon
48 response, which reflects different adaptive cellular processes. An
49 understanding of how coronavirus-elicited ER stress is actively involved in viral
50 replication and manipulates the host IFN-I response has remained elusive.
51 Here, TGEV inhibited host miR-30a-5p via the ER stress sensor IRE1 α , which
52 led to the increased expression of negative regulators of JAK-STAT signaling
53 cascades, namely, SOCS1 and SOCS3. Increased SOCS1 or SOCS3
54 expression impaired the IFN-I antiviral response, promoting TGEV replication.
55 These findings enhance our understanding of the strategies used by
56 coronaviruses to antagonize IFN-I innate immunity via IRE1 α -mediated
57 manipulation of the miR-30a-5p-SOCS axis, highlighting the crucial role of
58 IRE1 α in innate antiviral resistance and the potential of IRE1 α as a novel target
59 against coronavirus infection.

60

61 Introduction

62 Endoplasmic reticulum (ER) stress and the unfolded protein response
63 (UPR) are common consequences of coronavirus infection (1-5). Our groups
64 and others have demonstrated that coronaviruses, including severe acute
65 respiratory syndrome coronavirus (SARS-CoV), infectious bronchitis virus
66 (IBV), porcine epidemic diarrhea virus (PEDV), and transmissible
67 gastroenteritis virus (TGEV), are all capable of inducing significant ER stress
68 following infection and simultaneously trigger multiple UPR pathways to
69 restore ER homeostasis (1, 5-8). During ER stress, inositol-requiring enzyme 1
70 α (IRE1 α) is activated by oligomerization and autophosphorylation (9-11).
71 IRE1 α activation initiates diverse downstream signaling of the UPR either
72 through splicing of X-box binding protein 1 (XBP1) or through
73 posttranscriptional modifications via IRE1 α -dependent mRNA degradation
74 (RIDD) (9, 12). IRE1 α regulates genes involved in protein entry into the ER,
75 folding, glycosylation, and ER-associated degradation (ERAD) to facilitate ER
76 homeostasis (11, 13). Moreover, IRE1 α degrades ER-localized mRNAs via
77 RIDD to reduce the burden of protein entry into the ER (14). In addition to
78 degrading mRNA, activated IRE1 α has recently been demonstrated to cleave
79 precursor microRNAs (pre-miRNAs) and to degrade miRNAs during
80 noninfection-derived ER stress (15, 16). Given the crucial roles of IRE1 α
81 signaling in cellular fate determination, many RNA viruses, such as influenza A
82 virus (IAV) and Japanese encephalitis virus (JEV), employ IRE1 α signaling to
83 facilitate their replication (17, 18). However, whether and how IRE1 α
84 specifically modulates coronavirus replication are not well established.

85 Type I interferons (IFN-I) (IFN- α/β) play crucial roles in host antiviral
86 responses. Upon viral infection, host cells react quickly to the invading viruses
87 by synthesizing and secreting IFN-I. Binding of IFN-I to its receptor (interferon
88 alpha/beta receptor, IFNAR) results in activation of Janus family kinases (JAKs)
89 and the subsequent activation of signal transducer and activator of
90 transcription (STAT) signaling cascades, thereby inducing the expression of

91 IFN-stimulated genes (ISGs) (19). However, over the course of the long
92 evolutionary competition between viruses and host cells, coronaviruses have
93 evolved diverse mechanisms to counteract the IFN-I response (20-23). At least
94 11 viral proteins of coronavirus SARS-CoV and PEDV have been identified as
95 IFN-I antagonists (20, 23, 24). By contrast, TGEV induces high levels of IFN-I
96 *in vivo* and *in vitro* after infection (25-27). Despite a wealth of knowledge
97 regarding how TGEV triggers IFN-I production, how TGEV counters the
98 antiviral activity of IFN-I has not been fully elucidated.

99 microRNAs (miRNAs) are a large family of short (19-24 nucleotides)
100 noncoding RNAs that regulate gene expression posttranscriptionally through
101 translational repression and/or mRNA degradation by binding their seed
102 regions to complementary sites present in the 3' untranslated region (UTR) of
103 target genes (28, 29). Given the critical roles of miRNAs in regulating gene
104 expression, unsurprisingly, viruses take advantage of host miRNAs to target
105 vital components of the IFN-I response and impair IFN-I antiviral activity for
106 optimal infection (28, 30, 31). JEV evades IFN-I and enhances viral infection
107 by downregulating the expression of miR-432, which directly targets the
108 suppressor of cytokine signaling protein 5 (SOCS5), a negative regulator of the
109 JAK-STAT1 signaling cascade (32). Porcine reproductive and respiratory
110 syndrome virus (PRRSV) dampens the JAK-STAT signaling of IFN-I to
111 facilitate its replication via upregulating host miR-30c, which directly targets
112 JAK1 (30). However, the potential role of miRNAs in the coronavirus escape
113 from the IFN-I response has remained elusive.

114 Aberrant miRNA expression is integrally related to the progression and
115 pathogenesis of diseases (30, 33, 34). Although we have gained considerable
116 insights into aberrant miRNA expression by cis-regulatory elements and
117 trans-acting factors caused by viral infection, the contribution of the
118 virus-induced UPR to aberrant miRNA expression has rarely been investigated.
119 Recent studies have shown that activated IRE1 α affects cell fate by directly
120 degrading a subset of host miRNAs (miR-17, miR-34a, miR-96, and miR-125b)

121 under persistent ER stress induced by chemicals or noninfectious diseases
122 (15, 35). However, whether and how viruses exploit IRE1 α to manipulate
123 miRNA expression for optimal viral infection remain unknown.

124 In this study, TGEV infection downregulated the expression of host
125 miR-30a-5p via virally triggered IRE1 α -mediated UPR induction. miR-30a-5p
126 suppressed TGEV infection by enhancing the IFN-induced antiviral signaling
127 pathway by directly targeting the negative regulators of IFN signaling, SOCS1
128 and SOCS3. Moreover, TGEV infection *in vivo* suppressed miR-30a-5p
129 expression and significantly elevated the expression of SOCS1 and SOCS3 in
130 the ileum. Altogether, these data contribute new insights into the roles of
131 IRE1 α in regulating the innate immune response and help to explain how
132 TGEV escapes host IFN-I innate immunity.

133

134 Results

135 TGEV infection downregulates miR-30a-5p expression

136 The host miR-30 family (five members: miR30a-e) plays important roles in
137 cancers and viral infections (30, 34, 36, 37). We recently reported that
138 miR-30a-5p, a member of the miR-30 family, is downregulated and inversely
139 correlated with the levels of ER stress in renal cancer, indicating that ER stress
140 might inhibit miR-30a-5p expression (34). To assess whether ER stress
141 suppresses the expression of miR-30a-5p, we initially analyzed the levels of
142 miR-30a-5p in swine testicular (ST) cells following treatment with the ER stress
143 inducer thapsigargin (Tg). Tg treatment substantially diminished the
144 abundance of miR-30a-5p and exhibited a dose-dependent suppression (Fig.
145 1A), indicating that Tg-derived ER stress reduces miR-30a-5p abundance. Our
146 lab and others have shown that similar to other coronaviral infections, TGEV
147 infection triggers significant ER stress and initiates all three UPR pathways (1,
148 8). To explore whether miR-30a-5p could be regulated by TGEV infection, we
149 initially monitored miR-30a-5p expression in ST cells after TGEV infection with
150 different multiplicities of infection (MOIs). Compared with mock infection,

151 TGEV infection significantly reduced the levels of miR-30a-5p at 24 h
152 postinfection (hpi) and displayed a MOI-dependent response (Fig. 1B). To
153 determine the stage at which miR-30a-5p suppression by TGEV infection
154 occurs, we analyzed miR-30a-5p expression at different time points after
155 TGEV infection. TGEV infection with a MOI of 1 caused a typical cytopathic
156 effect (CPE) including syncytium in ST cells at 24 hpi and resulted in
157 approximately 35% cell death at 48 hpi. miR-30a-5p reduction occurred after
158 12 hpi and then gradually decreased up to 48 hpi (Fig. 1D), indicating that
159 TGEV infection decreases miR-30a-5p abundance at the late stage of infection.
160 TGEV infection in ST cells was confirmed by quantifying the viral genomes
161 (Fig. 1C and 1E). TGEV primarily infects villous epithelial cells in the small
162 intestine *in vivo* and causes watery diarrhea. To assess whether TGEV
163 infection also decreases miR-30a-5p expression *in vivo*, we quantified
164 miR-30a-5p expression in piglet ilea at 48 hpi. TGEV infection resulted in an
165 approximately 5-fold reduction in miR-30a-5p abundance in the ileum *in vivo*
166 (0.021 ± 0.003) compared with that in uninfected control ileum (0.096 ± 0.016)
167 ($p < 0.01$) (Fig. 1F). TGEV infection in the ileum was confirmed by quantifying
168 TGEV RNA (Fig. 1G). These results demonstrate that TGEV infection
169 decreases miR-30a-5p expression.

170

171 IRE1 α -mediated UPR induction inhibits miR-30a-5p expression

172 We next investigated the mechanisms responsible for the suppression of
173 miR-30a-5p by TGEV infection. In recent studies, IRE1 α , a highly conserved
174 ER stress sensor comprising a protein kinase and RNase, has the ability to
175 degrade miRNAs in addition to degrading mRNA under ER stress (35, 38, 39).
176 IRE1 α activation by TGEV infection was assessed by real-time polymerase
177 chain reaction (RT-PCR) and PstI digestion, which showed a recognition site
178 located within the 26-nt region of XBP1 cDNA removed by IRE1 α -mediated
179 splicing, as previously described (12, 40). Consistent with previous results for
180 the coronavirus mouse hepatitis virus (MHV) (41), TGEV infection caused

substantial cytoplasmic cleavage of the XBP1u transcript into the XBP1s transcription factor starting at 24 hpi, indicating that IRE1 α is activated by TGEV infection (Fig. 2A). IRE1 α activation was further confirmed by analyzing the expression of the XBP1s downstream target gene, namely, ER-localized DnaJ homologue 4 (ERdj4) (Fig. 2B). The activity of IRE1 α (the ratio of spliced XBP1 DNA to total XBP1u DNA) was inversely correlated with the levels of miR-30a-5p expression (Fig. 2A and 1D) ($R=0.933$, $p<0.01$). The decrease in miR-30a-5p expression primarily occurred within 24-48 hpi, the period in which significant IRE1 α activation was triggered by TGEV infection (Fig. 1D and 2A). These findings suggest that TGEV-induced IRE1 α activation may involve decreased miR-30a-5p expression during TGEV infection. To demonstrate that activated IRE1 α is responsible for the downregulation of miR-30a-5p, we monitored the expression of miR-30a-5p in TGEV-infected or Tg-treated cells after inhibiting IRE1 α function with 4 μ 8c, a highly specific and selective inhibitor of the RNase activity of IRE1 α (14). The effective blockage of IRE1 α RNase function by 4 μ 8c was confirmed by PCR analysis of XBP1 cleavage (Fig. 2C). The inhibition of IRE1 α RNase by 4 μ 8c almost completely abolished the suppression of miR-30a-5p by TGEV or Tg (Fig. 2D and 2E). To further verify the contribution of IRE1 α to miR-30a-5p expression, we knocked down IRE1 α expression by specific small interfering RNAs (siRNAs), and the efficiency of IRE1 α knockdown was confirmed by Western blotting (Fig. 2F). The silencing of IRE1 α by siRNAs significantly rescued the decreased miR-30a-5p induced by TGEV infection (Fig. 2G) or Tg treatment (Fig. 2H) ($p<0.05$). In addition, the efficiency of miR-30a-5p restored by IRE1 α siRNAs was correlated with the knockdown efficiency of IRE1 α siRNAs (Fig. 2F-2H). Taken together, these results show that activated IRE1 α reduces miR-30a-5p expression.

miR-30a-5p suppresses TGEV propagation

In agreement with our previous results, compared with control dimethyl

211 sulfoxide (DMSO) treatment, blocking IRE1 α with 4 μ 8c significantly reduced
212 TGEV replication, as revealed by measuring the quantities of viral genomes
213 (Fig. 3A) and infectious virions (Fig. 3B) (8). Consistent with 4 μ 8c treatment
214 results, knockdown of IRE1 α by silRE1 α #3, which was the most efficient at
215 silencing IRE1 α , significantly reduced the TGEV genome quantity and titer.
216 Both silRE1 α #1 and silRE1 α #2 also exhibited a tendency to decrease TGEV
217 propagation in ST cells but not significantly because of silencing efficiency (Fig.
218 3C and 3D). The observed levels of TGEV reduction were correlated with the
219 knockdown efficiency of IRE1 α siRNAs (Fig. 2F, 3C and 3D). These data
220 demonstrate that the IRE1 α pathway promotes TGEV replication.

221 Since TGEV replication was reduced after blocking IRE1 α signaling
222 cascades by 4 μ 8c or IRE1 α -specific silRE1 α #3, which rescued the
223 IRE1 α -mediated downregulation of miR-30a-5p expression, we reasoned that
224 miR-30a-5p may inhibit TGEV infection. To investigate the role of miR-30a-5p
225 in TGEV propagation, we monitored TGEV infection in ST cells after
226 transfecting miR-30a-5p mimics 24 h prior to infection. Compared with NC
227 mimics, miR-30a-5p mimics decreased the TGEV genome quantity and
228 progeny viral titer by up to 17-fold. The inhibition of TGEV by preexisting
229 miR-30a-5p mimics was dose dependent, and TGEV infection (MOI=0.01) was
230 substantially reduced by 80 nM and 160 nM miR-30a-5p mimics ($p<0.001$) (Fig.
231 3E and 3F). miR-30a-5p mimics also significantly decreased TGEV infection
232 when a MOI of 1 was used (data not shown). The suppression of TGEV
233 infection by miR-30a-5p was further confirmed by a TGEV nucleocapsid
234 protein immunofluorescence assay (IFA) (Fig. 3G). To determine the phase at
235 which preexisting miR-30a-5p overexpression suppresses TGEV infection, we
236 measured TGEV infection at different time points in the presence of
237 miR-30a-5p overexpression. miR-30a-5p significantly suppressed TGEV
238 replication at 24 and 36 hpi, indicating that miR-30a-5p-mediated reduction in
239 TGEV replication occurs at the late stage of TGEV infection (Fig. 3H).
240 Furthermore, the specific suppression of endogenous miR-30a-5p in ST cells

241 by the miR-30a-5p inhibitor boosted TGEV infection compared with that by the
242 inhibitor NC (Fig. 3I). These results demonstrate that miR-30a-5p suppresses
243 TGEV infection. To verify whether IRE1 α facilitates TGEV replication by
244 manipulating miR-30a-5p expression, we analyzed TGEV production in ST
245 cells transfected with a miR-30a-5p inhibitor in the presence of 4 μ 8c at 1.0
246 MOI of TGEV. The suppression of endogenous miR-30a-5p by the miR-30a-5p
247 inhibitor significantly abrogated 4 μ 8c-mediated TGEV suppression compared
248 with that by the DMSO mock control (Fig. 3I), indicating that IRE1 α facilitates
249 TGEV infection by manipulating miR-30a-5p expression. Taken together, our
250 data indicate that IRE1 α enhances TGEV replication by decreasing
251 miR-30a-5p abundance.

252

253 **miR-30a-5p enhances IFN-I antiviral signaling cascades rather than IFN-I** 254 **induction**

255 Next, we explored the mechanisms responsible for miR-30a-5p-mediated
256 TGEV inhibition. TGEV efficiently replicates in cells despite significant
257 amounts of endogenous IFN-I production after infection (25, 26), indicating
258 that some underlying mechanisms are exploited by TGEV to escape
259 IFN-I-induced antiviral responses. Given that miR-30a-5p inhibited TGEV
260 replication at the late stage of infection (Fig. 3H), we hypothesized that
261 miR-30a-5p suppresses TGEV replication possibly by enhancing IFN-I antiviral
262 signaling cascades rather than by promoting the production of IFN-I. To
263 exclude the possibility that miR-30a-5p enhances the production of IFN-I, we
264 initially analyzed IFN- β expression in ST cells following TGEV infection when
265 overexpressing miR-30a-5p. Consistent with previous studies (8, 25), TGEV
266 infection elicited a substantial amount of IFN- β production at 24 hpi (Fig. 4A).
267 Overexpression of miR-30a-5p did not significantly increase IFN- β production,
268 as measured by quantifying IFN- β protein levels following TGEV infection
269 relative to those observed in the presence of NC mimics (Fig. 4A), indicating
270 that miR-30a-5p does not modulate TGEV-induced IFN-I production.

271 The binding of IFN-I to the IFN-I receptor primarily activates the
272 JAK-STAT1 signaling pathway and induces hundreds of ISGs to inhibit viral
273 infection. To verify our hypothesis that miR-30a-5p hinders TGEV replication
274 largely by enhancing IFN-I antiviral signaling cascades, we initially monitored
275 the kinetic profiles of interferon-stimulated gene 15 (ISG15) expression
276 post-TGEV infection (Fig. 4B). The expression of ISG15 peaked at 24 hpi and
277 then significantly diminished, although IFN- β was continuously elevated during
278 the period from 24 to 48 hpi (Fig. 4B) ($P<0.05$). Consistent with the kinetic
279 profile of ISG15, STAT1 blotting results demonstrated that STAT1
280 phosphorylation peaked at 24 hpi and then decreased (Fig. 4C). These results
281 suggest that IFN-I antiviral signaling cascades are undermined during the later
282 stage of TGEV infection in contrast to IFN- β production. To directly verify if
283 TGEV infection impairs IFN-I antiviral signaling at the later stage of infection,
284 we stimulated TGEV-infected ST cells at 36 hpi by IFN- β for 30 min and
285 evaluated STAT1 activation. Compared with uninfected control cells,
286 TGEV-infected cells exhibited a significant reduction in IFN- β -elicited STAT1
287 phosphorylation (p-STAT1) (Fig. 4D), indicating that TGEV infection impairs
288 IFN-I antiviral signaling at a later stage. Furthermore, the time frame of the
289 observed decrease in ISG15 expression matched that of an observed
290 significant reduction in miR-30a-5p abundance during TGEV infection (Fig. 4B),
291 suggesting that miR-30a-5p may be relevant for the suppression of the IFN-I
292 antiviral response at the later stage of infection. To validate the role of
293 miR-30a-5p in modulating IFN-I antiviral signaling, we initially monitored the
294 activity of the IFN-stimulated response element (ISRE) with a luciferase assay
295 following IFN- β stimulation. Compared with NC mimics, MiR-30a-5p mimics
296 significantly enhanced the activity of ISRE stimulated by IFN- β ; in contrast,
297 compared with the NC inhibitor, the miR-30a-5p inhibitor suppressed
298 IFN- β -derived ISRE activity (Fig. 4E). We next measured the expression of
299 antiviral ISG genes (ISG15, 2'-5'-oligoadenylate synthetase-like (OASL), and
300 myxovirus resistance protein 1 (MxA)) in the presence of miR-30a-5p

301 overexpression during TGEV infection (Fig. 4F) or IFN- β stimulation (Fig. 4G).
302 Compared the NC mimic control, MiR-30a-5p overexpression greatly
303 upregulated the expression of antiviral ISG genes in response to either TGEV
304 infection or IFN- β stimulation (Fig. 4F and 4G). Consistent with the results of
305 ISRE luciferase and ISG expression assays, the overexpression of
306 miR-30a-5p significantly promoted p-STAT1, whereas the inhibition of
307 endogenous miR-30a-5p decreased p-STAT1 levels following IFN- β
308 stimulation or TGEV infection (Fig. 4H). These data demonstrate that
309 miR-30a-5p promotes IFN-I signaling. Overall, we conclude that miR-30a-5p
310 reinforces IFN-I antiviral signaling rather than IFN-I production.

311 Consistent with previously published results (42, 43), we demonstrated
312 that IFN- β substantially reduced TGEV infection and exhibited anti-TGEV
313 activity *in vitro* (Fig. 4I). In agreement with the result that miR-30a-5p
314 enhanced IFN-I antiviral signaling, compared with NC mimics, overexpression
315 of miR-30a-5p reduced TGEV infection and increased the efficiency of IFN- β in
316 inhibiting TGEV infection by more than 100-fold (Fig. 4I) ($p < 0.01$). The
317 inhibition of endogenous miR-30a-5p by the inhibitor significantly increased
318 TGEV infection and decreased the efficiency of IFN- β in suppressing TGEV
319 infection (Fig. 4I). Therefore, these data demonstrate that miR-30a-5p inhibits
320 TGEV replication by enhancing IFN-I antiviral signaling rather than through the
321 modulation of IFN-I production.

322

323 **miR-30a-5p directly targets SOCS1 and SOCS3**

324 To elucidate the underlying mechanisms by which miR-30a-5p enhances
325 IFN-I signaling, we performed computational analysis by using a TargetScan
326 prediction program to identify the potential target genes of miR-30a-5p. Since
327 miR-30a-5p promoted IFN-I signaling rather than IFN-I induction (Fig. 4), we
328 primarily focused on the target genes of miR-30a-5p that enhance IFN
329 signaling pathways. Computational analysis showed that miR-30a-5p could
330 potentially target SOCS1 and SOCS3 through a 3' UTR site that is conserved

331 in mammals (Fig. 5A). The SOCS family of proteins are endogenous potent
332 negative regulators of JAK-STAT signaling transduction (19, 44). Next, we
333 explored whether miR-30a-5p directly targets SOCS proteins and enhances
334 IFN-I signaling by downregulating SOCS expression. To verify whether
335 miR-30a-5p directly targets SOCS1 and SOCS3, we cloned the predicted
336 target sites in the 3' UTRs of SOCS1 or SOCS3 into a firefly luciferase reporter
337 vector. In addition, a mutant vector was constructed to eliminate possible
338 recognition by replacing five seed nucleotides (UGUUUAC to UAGGGUC) as
339 previously described (Fig. 5A) (30). Compared with the NC mimic treatment,
340 overexpression of miR-30a-5p in ST cells decreased the activity of the
341 luciferase reporter containing the SOCS1 or SOCS3 wild-type target sequence
342 but not that of the luciferase reporter containing the mutant target site of
343 SOCS1 or SOCS3. By contrast, compared with the NC inhibitor, the
344 miR-30a-5p inhibitor increased the activity of the luciferase reporter containing
345 the SOCS1 or SOCS3 wild-type target sequence but not that of the luciferase
346 reporter containing the mutant target site (Fig. 5B). These results confirm that
347 miR-30a-5p directly targets the 3' UTRs of SOCS1 and SOCS3. To further
348 verify SOCS1 and SOCS3 as direct targets of miR-30a-5p, we examined the
349 expression of SOCS1 and SOCS3 in ST cells transfected with miR-30a-5p
350 mimics or inhibitor. As expected, miR-30a-5p mimics significantly decreased
351 the transcript levels of SOCS1 and SOCS3 in ST cells (Fig. 5C). The
352 diminished expression of SOCS1 and SOCS3 induced by miR-30a-5p
353 overexpression was verified by Western blotting (Fig. 5D). Conversely,
354 compared with the NC inhibitor, the miR-30a-5p inhibitor increased the
355 expression of SOCS1 and SOCS3 in ST cells (Fig. 5C and 5D). The
356 modulation of miR-30a-5p abundance exerted an effect on the expression of
357 SOCS1 and SOCS3 in TGEV-infected ST cells similar to that in
358 TGEV-uninfected ST cells (Fig. 5D). Altogether, these data demonstrate that
359 miR-30a-5p downregulates the expression of SOCS1 and SOCS3 via directly
360 targeting their 3' UTRs.

361 TGEV infection downregulated miR-30a-5p expression through activation
362 of IRE1 α (Fig. 1 and 2). Reasonably, TGEV infection would upregulate the
363 expression of SOCS1 and SOCS3. As expected, TGEV infection substantially
364 elevated the expression of SOCS1 and SOCS3 in ST cells at 24 hpi and
365 exhibited a dose-dependent induction of MOIs (Fig. 5E). Furthermore, the
366 increased expression of SOCS1 and SOCS3 began at 12 hpi and was
367 substantially elevated at 24 hpi following TGEV infection as observed by
368 measuring both mRNA and protein levels, which was inversely correlated with
369 the kinetic expression profiles of miR-30a-5p (Fig. 5F and 5G). To further
370 validate the role of miR-30a-5p in manipulating SOCS1 and SOCS3
371 expression via IRE1 α , we assessed the expression of SOCS1 and SOCS3
372 after TGEV infection in the presence of 100 μ M 4 μ 8c pretreatment. Compared
373 with the DMSO-pretreated mock control, 4 μ 8c pretreatment strongly
374 decreased the expression of SOCS1 and SOCS3 in ST cells following TGEV
375 infection, and the reduction in SOCS1 and SOCS3 expression by 4 μ 8c was
376 counteracted by the miR-30a-5p inhibitor (Fig. 5H), indicating that TGEV
377 upregulates the expression of SOCS1 and SOCS3 through IRE1 α -mediated
378 modulation of miR-30a-5p expression. Consistent with the *in vitro* SOCS
379 expression results, the expression of both SOCS1 (Fig. 5I) and SOCS3 (Fig.
380 5J) in TGEV-infected ileum was also upregulated more than 10-fold. Taken
381 together, these data demonstrate that TGEV infection upregulates the
382 expression of SOCS1 and SOCS3 via IRE1 α -mediated modulation of
383 miR-30a-5p abundance.

384

385 **Increased expression of SOCS1 or SOCS3 disrupts the IFN-I antiviral**
386 **response and facilitates TGEV replication**

387 Because miR-30a-5p hindered TGEV infection (Fig. 3) and enhanced
388 IFN-I signaling (Fig. 4), next, we explored whether TGEV-derived suppression
389 of miR-30a-5p facilitates TGEV infection via modulation of IFN-I signaling by

390 SOCS1 and SOCS3. Initially, we analyzed the activation of the JAK-STAT1
391 pathway in response to IFN-I stimulation or TGEV infection of ST cells
392 transfected with pCAGGS-SOCS1, pCAGGS-SOCS3, or empty vector. The
393 expression of SOCS1 or SOCS3 was confirmed by an IFA (Fig. 6A). As
394 expected, the overexpression of SOCS1 or SOCS3 reduced p-STAT1 and the
395 ratio of p-STAT1 to total STAT1 in response to either IFN- β stimulation or
396 TGEV infection (Fig. 6B), indicating that the elevated expression of SOCS1 or
397 SOCS3 suppresses p-STAT1 induced by IFN- β or TGEV infection. Consistent
398 with the disruption of IFN-I-activated JAK-STAT1 signaling by either SOCS1 or
399 SOCS3, transient expression of SOCS1 substantially dampened the
400 anti-TGEV activity of IFN- β and enhanced TGEV infection as indicated by
401 quantification of TGEV genomes and viral titers, and the transient expression
402 of SOCS3 also dampened the anti-TGEV activity of IFN- β but significantly
403 elevated the levels of TGEV genomes only despite the trend of the increase in
404 TGEV titers (Fig. 6C). Importantly, the overexpression of either SOCS1 or
405 SOCS3 enhanced TGEV infection under physiological infection conditions in
406 the absence of IFN- β stimulation (Fig. 6D). Overexpression of SOCS1
407 suppressed p-STAT1, IFN- β antiviral activity, and TGEV infection more
408 efficiently than did overexpression of SOCS3 (Fig. 6B-6D). These results
409 demonstrate that the increased expression of SOCS1 and SOCS3 hinders
410 JAK-STAT1 signaling elicited by IFN-I or TGEV and enhances TGEV infection.
411 To further verify the roles of SOCS1 and SOCS3 in IFN-I anti-TGEV activity,
412 we silenced the expression of endogenous SOCS1 and SOCS3 using siRNAs.
413 The knockdown efficiency of SOCS1 siRNAs and SOCS3 siRNAs was
414 confirmed by Western blotting (Fig. 6E). By contrast, knockdown of
415 endogenous SOCS1 or SOCS3 by specific siRNAs in ST cells substantially
416 enhanced the anti-TGEV activity of IFN- β (Fig. 6F) and the expression of
417 IFN-I-induced ISGs (Fig. 6G). Overall, the silencing of endogenous SOCS1
418 and SOCS3 expression greatly decreased TGEV titers by up to 10-fold (Fig.
419 6H) and enhanced the expression of IFN-induced ISGs (Fig. 6I) in

420 non-IFN- β -stimulated ST cells compared with those in siRNA NC control cells.
421 In agreement with SOCS1 and SOCS3 overexpression results, the silencing of
422 SOCS1 enhanced the IFN- β -mediated antiviral response and hindered TGEV
423 infection more efficiently than did the knockdown of SOCS3 (Fig. 6E-6I),
424 suggesting that SOCS1 has a more important role in IFN-I signaling than does
425 SOCS3. Thus, these data collectively indicate that TGEV infection upregulates
426 the expression of SOCS1 and SOCS3, which undermines JAK-STAT1
427 signaling and facilitates TGEV infection.

428

429 **IRE1 α facilitates TGEV infection by modulating the miR-30a-5p/SOCS** 430 **axis**

431 We demonstrated above that TGEV-activated IRE1 α decreased the levels
432 of miR-30a-5p (Fig. 2) and that miR-30a-5p directly targeted SOCS family
433 proteins and downregulated their expression, which enhanced STAT1
434 activation and hindered TGEV infection (Figs. 3-6). To further verify whether
435 TGEV escapes the IFN-I response by disrupting the JAK-STAT1 pathway
436 through IRE1 α -mediated modulation of the miR-30a-5p/SOCS axis, we
437 initially monitored TGEV infection after inhibiting STAT1 with fludarabine (a
438 STAT1-specific inhibitor) in ST cells treated with 4 μ 8c. The suppression of
439 IRE1 α by 4 μ 8c promoted STAT1 activation, resulting in TGEV inhibition (Fig.
440 7A). The disruption of 4 μ 8c-mediated enhancement of STAT1 signaling by
441 fludarabine significantly rescued TGEV suppression by 4 μ 8c (Fig. 7A). In
442 agreement with these results, the overexpression of miR-30a-5p enhanced
443 STAT1 activation and hindered TGEV infection, and fludarabine-mediated
444 blockade of STAT1 activation significantly rescued the suppression of TGEV
445 infection by miR-30a-5p (Fig. 7C). The inhibition of STAT1 activation by
446 fludarabine was confirmed by Western blotting for p-STAT1 and total STAT1
447 (Fig. 7B and 7D). The rescue of 4 μ 8c or miR-30a-5p-mediated TGEV
448 inhibition by fludarabine treatment was not due to cellular cytotoxicity since
449 treatment with 4 μ 8c, fludarabine, or 4 μ 8c plus fludarabine did not cause

cellular cytotoxicity at the concentrations used in the study (Fig. 7E). These results suggest that IRE1 α enhances TGEV infection through miR-30a-5p/SOCS-mediated disruption of the JAK-STAT1 pathway. Finally, to directly verify whether the effect of the miR-30a-5p/SOCS axis on TGEV infection is dependent on the IFN-I antiviral response, we assessed the suppression of miR-30a-5p on TGEV in ST cells after knockdown of the IFN-I receptor IFNAR1. The silencing efficacy of IFNAR1 siRNAs was verified by measuring transcripts of IFNAR (Fig. 7F). Among the 3 tested siRNAs, only siIFNAR1#1 substantially silenced IFNAR1 expression (Fig. 7F). The silencing of IFNAR1 by siIFNAR1#1 compared with that by the siRNA control was further confirmed by the reduction in ISG expression (ISG15, OASL, and MxA) after IFN- β stimulation (Fig. 7G). Unlike the siRNA control, no inhibitory effect of miR-30a-5p on TGEV was observed in IFNAR1-silenced cells (Fig. 7H). In line with TGEV titer results, miR-30a-5p overexpression did not result in the enhancement of STAT1 activation in IFNAR1-silenced ST cells, whereas miR-30a-5p overexpression did in wild-type ST cells (Fig. 7I). These data demonstrate that miR-30a-5p overexpression suppresses TGEV infection via the IFN-I response. In summary, IRE1 α enhances TGEV infection through miR-30a-5p/SOCS axis-mediated escape from the IFN-I response.

Discussion

IFN-I has vital roles in the host innate immunity response against viral infections, and in turn, coronaviruses have evolved diverse strategies to counter the antiviral activity of IFN-I during infection (20, 23, 45). Coronavirus replication is structurally and functionally related to the ER, and ER stress is a common outcome in coronavirus-infected cells (1, 2, 45). The UPR constitutes a vital aspect of the virus-host interaction and modulates both viral replication and pathogenesis. However, an understanding of how UPR induction by coronaviruses actively participates in viral replication and manipulates the host

480 innate immune responses has remained elusive. In the present study, we
481 observed that TGEV infection induced the activation of IRE1 α , which facilitated
482 TGEV infection by modulating the miR-30a-5p/SOCS axis. Our results
483 revealed an unappreciated mechanism employed by TGEV to escape the
484 IFN-I antiviral response via IRE1 α -mediated modulation of the
485 miR-30a-5p/SOCS axis (Fig. 8).

486 IRE1 α , the most conserved UPR transducer with both kinase and RNase
487 activities, plays a critical role in restoring ER homeostasis (38, 46). Many
488 viruses have evolved strategies to employ IRE1 α signaling to facilitate their
489 infection. The inhibition of IRE1 α signaling by specific IRE1 α inhibitors or
490 siRNA decreases the replication of IAV, JEV and hepatitis C virus (HCV) (17,
491 18, 47). We also showed that the inhibition of IRE1 α by the specific inhibitor
492 4 μ 8c or by siRNA knockdown diminished TGEV replication *in vitro*, similar to
493 that observed for IAV, JEV and HCV. However, the mechanisms by which
494 IRE1 α facilitates viral infection remain elusive. IRE1 α may facilitate viral
495 infection by conferring resistance of the infected cells to apoptosis, as
496 observed for HCV (47). IRE1 α facilitates JEV replication by modulating viral
497 RNA translation through the RIDD pathway (18). In this study, we identified
498 another mechanism of IRE1 α enhancement of viral infection, which occurs
499 through reducing the endogenous abundance of miR-30a-5p. We also
500 observed that IRE1 α mediated the decrease in miR-125b and miR-125a levels
501 in Tg-treated ST cells (data not shown). Thus, the downregulation of
502 miR-30a-5p by IRE1 α is not specific to miR-30a-5p. This finding is consistent
503 with previous studies reporting that IRE1 α manipulates the expression of
504 subsets of cellular miRNAs, including miR-125b, miR-150, and miR-17, in
505 response to ER stress (15, 38, 47). However, the specificity and mechanisms
506 of IRE1 α -mediated manipulation of cellular miRNAs remain elusive and merit
507 further study.

508 In contrast to PEDV, which inhibits dsRNA-mediated IFN-I production (20),
509 TGEV infection results in very rapid and massive production of IFN-I *in vitro*

510 and *in vivo* (26, 27, 43, 48). Because TGEV infection is sensitive to IFN-I
511 activity, TGEV has several strategies to antagonize IFN-I signaling rather than
512 IFN-I production. This information is consistent with our finding that TGEV
513 impairs IFN-I JAK-STAT1 signaling at the late stage of infection (Fig. 4B-4D).
514 SOCS family proteins are negative regulators of cytokine-mediated JAK-STAT
515 signaling. Here, TGEV infection inhibited miR-30a-5p expression, resulting in
516 strongly upregulated expression of SOCS1 and SOCS3 (Figs. 1 and 5),
517 allowing efficient TGEV replication despite high IFN-I levels (Fig. 6).
518 Knockdown of the physiological expression levels of SOCS1 or SOCS3
519 resulted in up to a 4-fold increase in the expression of ISG15 and a more than
520 a 200-fold increase in the anti-TGEV activity of IFN-I (Fig. 6), indicating that
521 SOCS3 and especially SOCS1, which suppresses IFN-I signaling more
522 strongly than SOCS3, play vital roles in negatively regulating the IFN-I
523 response during TGEV infection. Our data indicate that TGEV largely evades
524 IFN-I innate immunity largely by modulating IFN-I antiviral signaling rather than
525 by manipulating the production of IFN-I. The induction of SOCS1 and SOCS3
526 to counteract IFN antiviral responses is also observed in other viruses, such as
527 SARS-CoV (49), herpes simplex virus type 1 (50), respiratory syncytial virus
528 (51), HCV (31), and IAV (52). SOCS1 and SOCS3 act on multiple STAT family
529 members and potently suppress both JAK-STAT1 and JAK-STAT3 signaling
530 pathways (53, 54). Thus, our study provides more evidence that SOCS family
531 proteins play a crucial role in antagonizing IFN-I responses during viral
532 infections.

533 Our results showed that miR-30a-5p enhanced IFN-I signaling and
534 significantly suppressed viral infection by directly targeting SOCS1 and
535 SOCS3 whose 3' UTRs are conserved in mammals (Fig. 5). Consistent with
536 our data, during the preparation of this article, a paper published by Zhen Xu
537 and colleagues revealed that miR-30a-5p directly targets the 3' UTR of SOCS3
538 and manipulates the expression of SOCS3 in mouse B cell lymphoma (55).
539 Importantly, we detected decreased expression of miR-30a-5p and increased

540 expression of SOCS1 and SOCS3 in TGEV-infected ileum. Reasonably, we
541 speculate that the miR-30a-5p/SOCS axis may have a role in TGEV
542 pathogenesis *in vivo*. Given that activation of IRE1 α and upregulation of SOCS
543 family proteins by many other viruses are not uncommon, the
544 IRE1 α -miR-30a-5p-SOCS axis may also be involved in the pathogenesis of
545 other viral infections, and further study is worthwhile.

546 In conclusion, here, we report a previously unappreciated mechanism by
547 which TGEV escapes IFN antiviral activity via IRE1 α -mediated miR-30a-5p
548 suppression and subsequent SOCS1 and SOCS3 upregulation (Fig. 8). Our
549 findings underscore the importance of IRE1 α in the regulation of IFN-I
550 signaling and TGEV infection, as well as broaden our knowledge regarding the
551 role of the UPR in aberrant host miRNA expression following viral infection. In
552 addition, our study sheds light on the crucial roles of SOCS1 and SOCS3 in
553 coronavirus infection.

554

555 **Materials and Methods**

556 **Cell culture, viruses and virus infection.** ST cells were cultured in
557 Dulbecco's Modified Eagle's Medium (DMEM; Gibco, USA) supplemented with
558 10% heat-inactivated fetal bovine serum (FBS; Gibco, USA), 100 U/mL
559 penicillin and 100 μ g/mL streptomycin in an incubator with 5% CO₂ at 37°C.
560 TGEV strain H87, derived from the virulent strain H16 (GenBank: FJ755618),
561 was propagated in ST cells. A TGEV stock was prepared and titrated as
562 previously described (56). For TGEV infection, ST cells were infected with
563 TGEV H87 at a desired MOI or mock infected with DMEM. After a 2-h
564 incubation at 37°C, cells were washed and cultured in DMEM supplemented
565 with 1% DMSO and 0.3% trypsin (0.25%, Gibco, USA) until harvested.

566 **Synthetic miRNAs, siRNAs, and transfection.** All miRNA mimics, miRNA
567 inhibitors, and siRNAs listed in Table 1 were designed and synthesized by
568 GenePharma (China). Cells were seeded for 16 h before transfection with
569 plasmid DNA or synthetic oligonucleotides using Lipofectamine 2000

570 (Invitrogen, USA) or Lipofectamine RNAiMAX (Invitrogen) according to the
571 manufacturer's protocol. The cells were infected with TGEV or stimulated by
572 IFN- β at 24 h after transfection. The cells were harvested for quantitative
573 real-time reverse transcription PCR (RT-qPCR) or Western blotting after a
574 24-h incubation.

575 **Chemical treatments.** Thapsigargin (Tg, a potent inducer of ER stress) and
576 4 μ 8c (a specific inhibitor of IRE1 α) (14) were purchased from Sigma-Aldrich,
577 and fludarabine (a STAT1 specific inhibitor) was purchased from Selleck. ST
578 cells were pretreated with different concentrations of chemicals or DMSO for 2
579 or 24 h, followed by inoculation with TGEV. After a 2-h incubation, the
580 supernatant was removed and replaced with culture media containing different
581 doses of chemicals. The samples were harvested for RT-qPCR and viral
582 titration at 24 hpi.

583 **RNA extraction, reverse transcription, and qPCR.** Total cellular RNA was
584 extracted using TRIzol (Thermo Fisher Scientific, USA) according to the
585 manufacturer's protocol. cDNA was prepared with a PrimeScript™ II 1st strand
586 cDNA synthesis kit (Takara, Japan). The expression pattern of each gene was
587 analyzed by RT-qPCR using a LightCycler480 II system (Roche, Swiss) as
588 previously described (56). For miRNA analyses, RNA was reverse transcribed
589 by using a miRNA First Strand cDNA Synthesis kit (Sangon Biotech, China),
590 and miRNA expression was assessed by RT-qPCR. PCR amplification was
591 performed in triplicate using the following conditions: 95°C for 10 min, followed
592 by 40 cycles of two steps (95°C for 15 s and 60°C for 40 s). The relative
593 expression levels of miRNAs were normalized to those of U6. The RNA
594 expression results are presented as the means \pm standard error of the mean
595 (SEM) from 3 independent experiments. The sequences of RT-qPCR primers
596 are listed in Table 2.

597 **microRNA target prediction and plasmid construction.** Target Scan 7.1
598 (<http://www.targetscan.org>) was used to predict SOCS1 and SOCS3 3' UTRs
599 as potential targets of miR-30a-5p. The 3' UTR of porcine SOCS1 (**GenBank:**

600 **GQ421919.1**) or SOCS3 (**GenBank: AY785557.1**) was amplified and inserted
601 into the pmirGLO luciferase reporter vector (Promega, USA) using Nhe I and
602 Xba I restriction sites. The mutant types of SOCS1 or SOCS3 3' UTR vectors
603 were constructed by mutating five seed nucleotides using a site-directed
604 mutagenesis kit (Stratagene, USA) according to the manufacturer's
605 instructions. To construct the SOCS1 and SOCS3 expression vectors, we
606 amplified the full-length CDS regions by specific primers, and the amplicons
607 were cloned into the vector pCAGGS-HA (Addgene) using EcoR I and Kpn I
608 restriction sites. The porcine ISRE reporter plasmid was kindly provided by
609 Prof. Wenhai Feng from China Agricultural University and was previously
610 described (30). All primers are listed in Table 2.

611 **Dual-luciferase reporter assays.** For miRNA target verification, wild-type or
612 mutant SOCS1 and SOCS3 3' UTR luciferase reporter vectors were
613 cotransfected with miR-30a-5p mimics, mimic NC, miR-30a-5p inhibitor, or
614 inhibitor NC (NC-i) into ST cells for 36 h. Furthermore, the ISRE reporter
615 plasmid and pRL-TK were cotransfected with either miR-30a-5p mimics, mimic
616 NC, inhibitor, or inhibitor NC for 24 h, followed by incubation with porcine IFN- β
617 (100 ng/mL) for 12 h. Next, the cells were collected for reporter activity testing
618 with a Dual-Luciferase Reporter Assay System (Promega, USA), according to
619 the manufacturer's protocol. All reporter assays were independently repeated
620 at least three times.

621 **Immunofluorescence assay (IFA).** IFAs were performed as previously
622 described (57). Briefly, ST cells were fixed with 4% paraformaldehyde and
623 permeabilized with 0.2% Triton X-100 and then blocked with blocking buffer for
624 2 h at 37°C. Cells were incubated with an anti-TGEV nucleocapsid monoclonal
625 antibody (1:1000) stocked in our laboratory or an anti-HA monoclonal antibody
626 (Sigma-Aldrich, 1:5000) at 37°C for 2 h. The cells were then labeled with an
627 Alexa Fluor 546 goat anti-mouse immunoglobulin G (IgG) antibody (1:500)
628 (Thermo Fisher Scientific, USA) for 1 h at 37°C. Cellular nuclei were stained
629 with 4',6-diamidino-2-phenylindole (DAPI) (1:100). Stained cells were

630 visualized using an AMG EVOS F1 fluorescence microscope.

631 **ELISA.** Culture supernatants were collected from treated cells at the indicated
632 times and stored at -80°C until testing. IFN- β protein levels in culture
633 supernatants were determined by porcine IFN- β enzyme-linked
634 immunosorbent assay (ELISA) kits (Bio-Swamp, China) according to the
635 manufacturer's instructions.

636 **Protein extraction and Western blotting.** To analyze the levels of host
637 IRE1 α , phospho-STAT1, STAT1, SOCS1, SOCS3 proteins, we analyzed the
638 cellular lysate by Western blotting as previously described (56). Briefly, ST
639 cells were lysed with Nonidet P-40 (NP-40) lysis buffer (Beyotime, China)
640 supplemented with cocktail protease inhibitor (Roche). Protein concentrations
641 of the supernatant fraction were measured with a bicinchoninic acid (BCA)
642 assay kit (Beyotime, China) and were equalized with extraction reagent. Equal
643 amounts of proteins were separated by sodium dodecyl sulfate-polyacrylamide
644 gel electrophoresis (SDS-PAGE) gels and transferred onto a nitrocellulose
645 membrane (GE Healthcare, USA). Membranes were blocked and incubated
646 with the corresponding primary antibody at 4°C overnight. The primary
647 antibodies used are as follows: β -actin (Sigma-Aldrich, 1:5000), SOCS1
648 (Sigma-Aldrich, 1:500), SOCS3 (CST, 1:1000), phospho-STAT1 (Abcam,
649 1:1000), STAT1 (Abcam, 1:1000) and IRE1 α (Santa Cruz Biotechnology,
650 1:500). After washing, the membrane was incubated with horseradish
651 peroxidase (HRP)-conjugated anti-mouse IgG or anti-rabbit IgG for 1 h at room
652 temperature. Then, immunolabeled proteins were visualized using
653 electrochemiluminescence (ECL) reagent (Thermo Fisher Scientific). The
654 intensity of each band was analyzed using ImageJ.

655 **TGEV infection of piglets.** Twelve two-day-old specific pathogen free (SPF)
656 piglets were randomly divided into two groups. Piglets in group one were orally
657 inoculated with 5 mL 1×10^5 TCID₅₀ TGEV H87 strain. After viral infection,
658 clinical signs were recorded on a daily basis. All piglets were euthanized at 48
659 hpi. Piglet small intestine samples were collected for RT-qPCR analyses. The

660 TGEV infection experiment was approved by the Animal Care and Ethics
661 Committee of Harbin veterinary research institute.

662 **Cellular cytotoxicity assay.** ST cells were cultured in 96-well plates for 24 h,
663 followed by incubation with Tg, 4 μ 8c, fludarabine, 4 μ 8c plus fludarabine, or the
664 same volume of DMSO for 24 h or 48 h. Next, cellular cytotoxicity assays were
665 performed using a Cell Counting Kit-8 (CCK-8) assay as previously described
666 (56).

667 **Statistical analysis.** All results in figures are presented, where appropriate, as
668 the means \pm SEM from three independent experiments and were analyzed in
669 GraphPad Prism (GraphPad Software, Inc). Differences were considered
670 significant if the *p* value was <0.05. The *p* values are indicated as follows:
671 **p*<0.05, ***p*<0.01, ****p*<0.001.

673 Acknowledgments

674 This work was supported by grants from the National Key R & D Program
675 of China (2016YFD0500100 and 2017YFD0502200) and the Heilongjiang
676 Science Fund for Study Abroad Returnees (LC2015013). The funders had no
677 role in the study design, data collection and analysis, decision to publish, or
678 preparation of the manuscript.

680 References

- 681 1. Cruz JL, Sola I, Becares M, Alberca B, Plana J, Enjuanes L, Zuniga S. 2011. Coronavirus gene 7
682 counteracts host defenses and modulates virus virulence. *PLoS pathogens* 7:e1002090.
- 683 2. Fung TS, Liu DX. 2014. Coronavirus infection, ER stress, apoptosis and innate immunity.
684 *Frontiers in microbiology* 5:296.
- 685 3. Favreau DJ, Desforjes M, St-Jean JR, Talbot PJ. 2009. A human coronavirus OC43 variant
686 harboring persistence-associated mutations in the S glycoprotein differentially induces the
687 unfolded protein response in human neurons as compared to wild-type virus. *Virology*
688 395:255-267.
- 689 4. Versteeg GA, van de Nes PS, Bredenbeek PJ, Spaan WJ. 2007. The coronavirus spike protein
690 induces endoplasmic reticulum stress and upregulation of intracellular chemokine mRNA
691 concentrations. *Journal of virology* 81:10981-10990.
- 692 5. DeDiego ML, Nieto-Torres JL, Jimenez-Guardeno JM, Regla-Nava JA, Alvarez E, Oliveros JC,
693 Zhao J, Fett C, Perlman S, Enjuanes L. 2011. Severe acute respiratory syndrome coronavirus

- 694 envelope protein regulates cell stress response and apoptosis. *PLoS pathogens* **7**:e1002315.
- 695 6. **Liao Y, Fung TS, Huang M, Fang SG, Zhong Y, Liu DX.** 2013. Upregulation of CHOP/GADD153
696 during coronavirus infectious bronchitis virus infection modulates apoptosis by restricting
697 activation of the extracellular signal-regulated kinase pathway. *Journal of virology*
698 **87**:8124-8134.
- 699 7. **Wang Y, Li JR, Sun MX, Ni B, Huan C, Huang L, Li C, Fan HJ, Ren XF, Mao X.** 2014. Triggering
700 unfolded protein response by 2-Deoxy-D-glucose inhibits porcine epidemic diarrhea virus
701 propagation. *Antiviral research* **106**:33-41.
- 702 8. **Xue M, Fu F, Ma Y, Zhang X, Li L, Feng L, Liu P.** 2018. The PERK Arm of the Unfolded Protein
703 Response Negatively Regulates Transmissible Gastroenteritis Virus Replication by Suppressing
704 Protein Translation and Promoting Type I Interferon Production. *Journal of virology* **92**.
- 705 9. **Oikawa D, Tokuda M, Hosoda A, Iwawaki T.** 2010. Identification of a consensus element
706 recognized and cleaved by IRE1 alpha. *Nucleic Acids Res* **38**:6265-6273.
- 707 10. **Fung TS, Liao Y, Liu DX.** 2014. The endoplasmic reticulum stress sensor IRE1alpha protects
708 cells from apoptosis induced by the coronavirus infectious bronchitis virus. *Journal of virology*
709 **88**:12752-12764.
- 710 11. **Safra M, Ben-Hamo S, Kenyon C, Henis-Korenblit S.** 2013. The ire-1 ER stress-response
711 pathway is required for normal secretory-protein metabolism in *C. elegans*. *Journal of cell*
712 *science* **126**:4136-4146.
- 713 12. **Calfon M, Zeng H, Urano F, Till JH, Hubbard SR, Harding HP, Clark SG, Ron D.** 2002. IRE1
714 couples endoplasmic reticulum load to secretory capacity by processing the XBP-1 mRNA.
715 *Nature* **415**:92-96.
- 716 13. **Kimmig P, Diaz M, Zheng J, Williams CC, Lang A, Aragon T, Li H, Walter P.** 2012. The unfolded
717 protein response in fission yeast modulates stability of select mRNAs to maintain protein
718 homeostasis. *eLife* **1**:e00048.
- 719 14. **Cross BC, Bond PJ, Sadowski PG, Jha BK, Zak J, Goodman JM, Silverman RH, Neubert TA,**
720 **Baxendale IR, Ron D, Harding HP.** 2012. The molecular basis for selective inhibition of
721 unconventional mRNA splicing by an IRE1-binding small molecule. *Proceedings of the*
722 *National Academy of Sciences of the United States of America* **109**:E869-878.
- 723 15. **Heindryckx F, Binet F, Ponticos M, Rombouts K, Lau J, Kreuger J, Gerwins P.** 2016.
724 Endoplasmic reticulum stress enhances fibrosis through IRE1alpha-mediated degradation of
725 miR-150 and XBP-1 splicing. *EMBO Mol Med* **8**:729-744.
- 726 16. **Belmadani S, Matrougui K.** 2017. The Unraveling Truth About IRE1 and MicroRNAs in
727 Diabetes. *Diabetes* **66**:23-24.
- 728 17. **Hassan IH, Zhang MS, Powers LS, Shao JQ, Baltrusaitis J, Rutkowski DT, Legge K, Monick**
729 **MM.** 2012. Influenza A viral replication is blocked by inhibition of the inositol-requiring
730 enzyme 1 (IRE1) stress pathway. *J Biol Chem* **287**:4679-4689.
- 731 18. **Bhattacharyya S, Sen U, Vratil S.** 2014. Regulated IRE1-dependent decay pathway is activated
732 during Japanese encephalitis virus-induced unfolded protein response and benefits viral
733 replication. *J Gen Virol* **95**:71-79.
- 734 19. **Porritt RA, Hertzog PJ.** 2015. Dynamic control of type I IFN signalling by an integrated
735 network of negative regulators. *Trends in immunology* **36**:150-160.
- 736 20. **Zhang Q, Yoo D.** 2016. Immune evasion of porcine enteric coronaviruses and viral modulation
737 of antiviral innate signaling. *Virus research* **226**:128-141.

- 738 21. **Menachery VD, Eisfeld AJ, Schafer A, Josset L, Sims AC, Proll S, Fan S, Li C, Neumann G,**
739 **Tilton SC, Chang J, Gralinski LE, Long C, Green R, Williams CM, Weiss J, Matzke MM,**
740 **Webb-Robertson BJ, Schepmoes AA, Shukla AK, Metz TO, Smith RD, Waters KM, Katze MG,**
741 **Kawaoka Y, Baric RS.** 2014. Pathogenic influenza viruses and coronaviruses utilize similar and
742 contrasting approaches to control interferon-stimulated gene responses. *mBio*
743 **5:e01174-01114.**
- 744 22. **Kindler E, Gil-Cruz C, Spanier J, Li Y, Wilhelm J, Rabouw HH, Zust R, Hwang M, V'Kovski P,**
745 **Stalder H, Marti S, Habjan M, Cervantes-Barragan L, Elliot R, Karl N, Gaughan C, van**
746 **Kuppeveld FJ, Silverman RH, Keller M, Ludewig B, Bergmann CC, Ziebuhr J, Weiss SR,**
747 **Kalinke U, Thiel V.** 2017. Early endonuclease-mediated evasion of RNA sensing ensures
748 efficient coronavirus replication. *PLoS pathogens* **13:e1006195.**
- 749 23. **Kamitani W, Narayanan K, Huang C, Lokugamage K, Ikegami T, Ito N, Kubo H, Makino S.**
750 2006. Severe acute respiratory syndrome coronavirus nsp1 protein suppresses host gene
751 expression by promoting host mRNA degradation. *Proceedings of the National Academy of*
752 *Sciences of the United States of America* **103:12885-12890.**
- 753 24. **Kopecky-Bromberg SA, Martinez-Sobrido L, Frieman M, Baric RA, Palese P.** 2007. Severe
754 acute respiratory syndrome coronavirus open reading frame (ORF) 3b, ORF 6, and
755 nucleocapsid proteins function as interferon antagonists. *Journal of virology* **81:548-557.**
- 756 25. **Zhou Y, Wu W, Xie L, Wang D, Ke Q, Hou Z, Wu X, Fang Y, Chen H, Xiao S, Fang L.** 2017.
757 Cellular RNA Helicase DDX1 Is Involved in Transmissible Gastroenteritis Virus nsp14-Induced
758 Interferon-Beta Production. *Frontiers in immunology* **8:940.**
- 759 26. **Riffault S, Carrat C, van Reeth K, Pensaert M, Charley B.** 2001. Interferon-alpha-producing
760 cells are localized in gut-associated lymphoid tissues in transmissible gastroenteritis virus
761 (TGEV) infected piglets. *Veterinary research* **32:71-79.**
- 762 27. **Becares M, Pascual-Iglesias A, Nogales A, Sola I, Enjuanes L, Zuniga S.** 2016. Mutagenesis of
763 Coronavirus nsp14 Reveals Its Potential Role in Modulation of the Innate Immune Response.
764 *Journal of virology* **90:5399-5414.**
- 765 28. **Forster SC, Tate MD, Hertzog PJ.** 2015. MicroRNA as Type I Interferon-Regulated Transcripts
766 and Modulators of the Innate Immune Response. *Frontiers in immunology* **6:334.**
- 767 29. **O'Neill LA, Sheedy FJ, McCoy CE.** 2011. MicroRNAs: the fine-tuners of Toll-like receptor
768 signalling. *Nature reviews. Immunology* **11:163-175.**
- 769 30. **Zhang Q, Huang C, Yang Q, Gao L, Liu HC, Tang J, Feng WH.** 2016. MicroRNA-30c Modulates
770 Type I IFN Responses To Facilitate Porcine Reproductive and Respiratory Syndrome Virus
771 Infection by Targeting JAK1. *J Immunol* **196:2272-2282.**
- 772 31. **Xu G, Yang F, Ding CL, Wang J, Zhao P, Wang W, Ren H.** 2014. MiR-221 accentuates IFNs
773 anti-HCV effect by downregulating SOCS1 and SOCS3. *Virology* **462-463:343-350.**
- 774 32. **Sharma N, Kumawat KL, Rastogi M, Basu A, Singh SK.** 2016. Japanese Encephalitis Virus
775 exploits the microRNA-432 to regulate the expression of Suppressor of Cytokine Signaling
776 (SOCS) 5. *Sci Rep* **6:27685.**
- 777 33. **Trobaugh DW, Klimstra WB.** 2017. MicroRNA Regulation of RNA Virus Replication and
778 Pathogenesis. *Trends in molecular medicine* **23:80-93.**
- 779 34. **Wang C, Cai L, Liu J, Wang G, Li H, Wang X, Xu W, Ren M, Feng L, Liu P, Zhang C.** 2017.
780 MicroRNA-30a-5p Inhibits the Growth of Renal Cell Carcinoma by Modulating GRP78
781 Expression. *Cellular physiology and biochemistry : international journal of experimental*

- cellular physiology, biochemistry, and pharmacology **43**:2405-2419.
35. **Upton JP, Wang L, Han D, Wang ES, Huskey NE, Lim L, Truitt M, McManus MT, Ruggero D, Goga A, Papa FR, Oakes SA.** 2012. IRE1alpha cleaves select microRNAs during ER stress to derepress translation of proapoptotic Caspase-2. *Science* **338**:818-822.
36. **Jia Z, Wang K, Wang G, Zhang A, Pu P.** 2013. MiR-30a-5p antisense oligonucleotide suppresses glioma cell growth by targeting SEPT7. *PloS one* **8**:e55008.
37. **Fu Y, Xu W, Chen D, Feng C, Zhang L, Wang X, Lv X, Zheng N, Jin Y, Wu Z.** 2015. Enterovirus 71 induces autophagy by regulating has-miR-30a expression to promote viral replication. *Antiviral research* **124**:43-53.
38. **Hassler J, Cao SS, Kaufman RJ.** 2012. IRE1, a double-edged sword in pre-miRNA slicing and cell death. *Dev Cell* **23**:921-923.
39. **Emde A, Eitan C, Liou LL, Libby RT, Rivkin N, Magen I, Reichenstein I, Oppenheim H, Eilam R, Silvestroni A, Alajajian B, Ben-Dov IZ, Aebischer J, Savidor A, Levin Y, Sons R, Hammond SM, Ravits JM, Moller T, Hornstein E.** 2015. Dysregulated miRNA biogenesis downstream of cellular stress and ALS-causing mutations: a new mechanism for ALS. *The EMBO journal* **34**:2633-2651.
40. **Yu CY, Hsu YW, Liao CL, Lin YL.** 2006. Flavivirus infection activates the XBP1 pathway of the unfolded protein response to cope with endoplasmic reticulum stress. *Journal of virology* **80**:11868-11880.
41. **Bechill J, Chen Z, Brewer JW, Baker SC.** 2008. Coronavirus infection modulates the unfolded protein response and mediates sustained translational repression. *Journal of virology* **82**:4492-4501.
42. **Jordan LT, Derbyshire JB.** 1995. Antiviral action of interferon-alpha against porcine transmissible gastroenteritis virus. *Veterinary microbiology* **45**:59-70.
43. **Zhu L, Yang X, Mou C, Yang Q.** 2017. Transmissible gastroenteritis virus does not suppress IFN-beta induction but is sensitive to IFN in IPEC-J2 cells. *Veterinary microbiology* **199**:128-134.
44. **Vlotides G, Sorensen AS, Kopp F, Zitzmann K, Cengic N, Brand S, Zachoval R, Auernhammer CJ.** 2004. SOCS-1 and SOCS-3 inhibit IFN-alpha-induced expression of the antiviral proteins 2,5-OAS and MxA. *Biochem Biophys Res Commun* **320**:1007-1014.
45. **Minakshi R, Padhan K, Rani M, Khan N, Ahmad F, Jameel S.** 2009. The SARS Coronavirus 3a protein causes endoplasmic reticulum stress and induces ligand-independent downregulation of the type 1 interferon receptor. *PloS one* **4**:e8342.
46. **Credle JJ, Finer-Moore JS, Papa FR, Stroud RM, Walter P.** 2005. On the mechanism of sensing unfolded protein in the endoplasmic reticulum. *Proceedings of the National Academy of Sciences of the United States of America* **102**:18773-18784.
47. **Fink SL, Jayewickreme TR, Molony RD, Iwawaki T, Landis CS, Lindenbach BD, Iwasaki A.** 2017. IRE1alpha promotes viral infection by conferring resistance to apoptosis. *Science signaling* **10**.
48. **Charley B, Laude H.** 1988. Induction of alpha interferon by transmissible gastroenteritis coronavirus: role of transmembrane glycoprotein E1. *Journal of virology* **62**:8-11.
49. **Okabayashi T, Kariwa H, Yokota S, Iki S, Indoh T, Yokosawa N, Takashima I, Tsutsumi H, Fujii N.** 2006. Cytokine regulation in SARS coronavirus infection compared to other respiratory virus infections. *Journal of medical virology* **78**:417-424.

- 826 50. **Yokota S, Yokosawa N, Okabayashi T, Suzutani T, Miura S, Jimbow K, Fujii N.** 2004. Induction
827 of suppressor of cytokine signaling-3 by herpes simplex virus type 1 contributes to inhibition
828 of the interferon signaling pathway. *Journal of virology* **78**:6282-6286.
- 829 51. **Zheng J, Yang P, Tang Y, Pan Z, Zhao D.** 2015. Respiratory Syncytial Virus Nonstructural
830 Proteins Upregulate SOCS1 and SOCS3 in the Different Manner from Endogenous IFN
831 Signaling. *J Immunol Res* **2015**:738547.
- 832 52. **Pauli EK, Schmolke M, Wolff T, Viemann D, Roth J, Bode JG, Ludwig S.** 2008. Influenza A
833 virus inhibits type I IFN signaling via NF-kappaB-dependent induction of SOCS-3 expression.
834 *PLoS pathogens* **4**:e1000196.
- 835 53. **Babon JJ, Kershaw NJ, Murphy JM, Varghese LN, Laktyushin A, Young SN, Lucet IS, Norton
836 RS, Nicola NA.** 2012. Suppression of cytokine signaling by SOCS3: characterization of the
837 mode of inhibition and the basis of its specificity. *Immunity* **36**:239-250.
- 838 54. **Yang Y, Yang L, Liang X, Zhu G.** 2015. MicroRNA-155 Promotes Atherosclerosis Inflammation
839 via Targeting SOCS1. *Cellular physiology and biochemistry : international journal of*
840 *experimental cellular physiology, biochemistry, and pharmacology* **36**:1371-1381.
- 841 55. **Xu Z, Ji J, Xu J, Li D, Shi G, Liu F, Ding L, Ren J, Dou H, Wang T, Hou Y.** 2017. MiR-30a increases
842 MDSC differentiation and immunosuppressive function by targeting SOCS3 in mice with B-cell
843 lymphoma. *FEBS J* **284**:2410-2424.
- 844 56. **Xue M, Zhao J, Ying L, Fu F, Li L, Ma Y, Shi H, Zhang J, Feng L, Liu P.** 2017. IL-22 suppresses the
845 infection of porcine enteric coronaviruses and rotavirus by activating STAT3 signal pathway.
846 *Antiviral research* **142**:68-75.
- 847 57. **Fu F, Li L, Shan L, Yang B, Shi H, Zhang J, Wang H, Feng L, Liu P.** 2017. A spike-specific
848 whole-porcine antibody isolated from a porcine B cell that neutralizes both genogroup 1 and
849 2 PEDV strains. *Veterinary microbiology* **205**:99-105.

850

851

852 **Table 1 Sequences of miRNA mimics, inhibitors, and siRNAs**

Small RNA	Sequence (5'-3')
miR-30a-5p	UGUAAACAUCUCGACUGGAAG
miR-30a-5p inhibitor	CUUCCAGUCGAGGAUGUUUACA
silRE1 α #1	GCACAGACCUGAAGUUCAATT
silRE1 α #2	GGAGGUUAUCGACCUGGUUTT
silRE1 α #3	CCAUCAUCCUGAGCACCUUTT
siSOCS1#1	CCUGCACGGAGCAUUAACUTT
siSOCS1#2	UCUUCGCCCUCAGUGUGAATT
siSOCS1#3	GCCGACAAUGCAAUCUCCATT
siSOCS3#1	UCAAGCUGGUGCGUCACUATT
siSOCS3#2	CCUGGACUCCUAUGAGAAATT
siSOCS3#3	UCUUCACGCUCAGCGUCAATT
silFNAR1#1	CCAGCUUUACCCACUAAUUTT
silFNAR1#2	CCGGGUCUAUGUUCUAAAATT
silFNAR1#3	GCCUGGAUGUCAAU AUGUUTT

853

854

855

856

857

858

859

860

861

862

863

864

865

866 Table 2 Sequences of primers used in the present study

Primer	Sequences (5'-3')
miR-30a-5p-qPCR-F	TGTAAACATCCTCGACTGGAAG
Uni-miR-qPCR-R	GCGAGCACAGAATTAATACGACTCAC
ISG15-qPCR-F	AGC ATG GTC CTG TTG ATG GTG
ISG15-qPCR-R	CAG AAA TGG TCA GCT TGC ACG
MxA-qPCR-F	CACTGCTTTGATACAAGGAGAGG
MxA-qPCR-R	GCACTCCATCTGCAGAACTCAT
OASL-qPCR-F	TCCCTGGGAAGAATGTGCAG
OASL-qPCR-R	CCCTGGCAAGAGCATAGTGT
SOCS1-qPCR-F	CGCCCTCAGTGTGAAGATGG
SOCS1-qPCR-R	GCTCGAAGAGGCAGTCGAAG
SOCS3-qPCR-F	CACTCTCCAGCATCTCTGTC
SOCS3-qPCR-R	TCGTAAGTGGTCCAGGAAGT
TGEV-qPCR-F	GCTTGATGAATTGAGTGCTGATG
TGEV-qPCR-R	CCTAACCTCGGCTTGTCTGG
GAPDH-qPCR-F	CCTTCCGTGTCCCTACTGCCAAC
GAPDH-qPCR-R	GACGCCTGCTTCACCACTTCT
IFN- β -qPCR-F	AGCACTGGCTGGAATGAAAC
IFN- β -qPCR-R	TCCAGGATTGTCTCCAGGTC
ERdj4-qPCR-F	CAGAGAGATTGCAGAAGCATATGA
ERdj4-qPCR-R	GCTTCTTGGATCGAGTGTCTTG
IFNAR1-qPCR-F	ACATCACCTGCCTTCACCAG
IFNAR1-qPCR-R	CATGGAGCCACTGAGCTTGA
XBP1-F	AAACAGAGTAGCAGCTCAGACTGC
XBP1-R	GAATCTCTAAGACTAGGGGCTTTGTA
SOCS1-EcoR I-F	CGGAATTCATGGTAGCACACAACCAGGTG
SOCS1-Kpn I-R	GGGGTACCTCATATCTGGAAGGGGAAGGAG
SOCS3-EcoR I-F	CGGAATTCATGGTCACCCACAGCAAGTTC
SOCS3-Kpn I-R	GGGGTACCTTAAAGTGGGGCATCGTACTGC
SOCS1-3' UTR-Nhe I-F	CTAGCTAGCATTATTTCTTGAACCATGTG
SOCS1-3' UTR-Xba I-R	GCTCTAGACACAGCAGAAAAATAAAGCCAG
SOCS3-3' UTR-Nhe I-F	CTAGCTAGCTTCTATTTTGTGCCTCCTGAC
SOCS3-3' UTR-Xba I-R	GCTCTAGAGTTTGACTTGGATTGGTATTTT
SOCS1-3' UTR-MT-F	CTTCATAGGGTCATATACCCAGTATCTTTGCACAAAC
SOCS1-3' UTR-MT-R	TATATGACCCTATGAAGAGGTAGGAGGTACTGAGTTC
SOCS3-3' UTR-MT-F	ATAATAGGGTCAATCTGCCTCAATCACTCTGTCTTTTA
SOCS3-3' UTR-MT-R	TTGACCCTATTATTAACCAACAAACAAACCCAAAC

867

868

Figure legends

Fig. 1. TGEV infection suppresses miR-30a-5p expression *in vitro* and *in vivo*.

(A). The ER stress inducer Tg decreased miR-30a-5p expression in ST cells. The miR-30a-5p levels in ST cells were measured by RT-qPCR after Tg treatment for 24 h. (B-E). TGEV infection downregulated miR-30a-5p expression *in vitro*. The miR-30a-5p levels (B) and TGEV infection (C) in ST cells were measured by RT-qPCR at 24 hpi with different MOIs. For time kinetics, the levels of miR-30a-5p (D) and TGEV genomes (E) in ST cells were quantified at the indicated time points after infection with TGEV at a MOI of 1. The results from three independent experiments are shown. (F, G). TGEV infection suppressed miR-30a-5p expression *in vivo*. Piglets were orally inoculated with 5 mL 1×10^5 TCID₅₀ TGEV or DMEM. Total cellular RNA from each ileum was collected at 48 hpi, and the levels of miR-30a-5p (F) and TGEV viral RNA in ileum (G) were measured by RT-qPCR. *, $p < 0.05$; **, $p < 0.01$; ***, $p < 0.001$ vs. mock-infected control.

Fig. 2. Activated IRE1 α reduces miR-30a-5p abundance. (A). Analysis of IRE1 α activation by XBP1 mRNA splicing. IRE1 α activation by TGEV infection was analyzed by PCR amplification of total XBP1 cDNA and further digestion with Pst1 as previously described (40). The sizes of the PCR-amplified fragments from spliced and unspliced XBP1 DNA with or without Pst1 cleavage are also listed. The PCR fragments of total XBP1, spliced and unspliced XBP1 DNA in ST cells that were infected with TGEV at a MOI of 1 for various time points or treated with Tg (1 μ M) for 24 h are shown. The PCR products of the housekeeping gene GAPDH are shown in the top panel as an internal control. The ratio of the band intensities for spliced and total XBP1 DNA in the infected cells was normalized to that of the mock-infected cells. (B). TGEV infection upregulated ERdj4 expression. The relative expression of ERdj4 to GAPDH following TGEV infection was measured and presented. (C). Analysis of IRE1 α activation in partial samples from A, D, or E. (D-E). The inhibition of IRE1 α by

899 4 μ 8c rescued the suppression of miR-30a-5p by TGEV (D) or Tg (E). ST cells
900 were pretreated with 50 or 100 μ M 4 μ 8c for 2 h followed by TGEV infection
901 (MOI=1) (D) or Tg (1 μ M) (E). The relative expression of miR-30a-5p to internal
902 U6 siRNA was measured by RT-qPCR after 24 h. The results are presented as
903 the relative expression of miR-30a-5p in ST cells normalized to that of
904 miR-30a-5p in the mock control cells. (F-H). Knockdown of IRE1 α rescued
905 miR-30a-5p suppression following TGEV infection or Tg treatment. ST cells
906 were transfected with siIRE1 α #1, siIRE1 α #2, siIRE1 α #3, or siRNA scrambled
907 control at 100 nM for 24 h, followed by infection with TGEV for 24 h at a MOI of
908 0.01 (F and G) or treatment with Tg (1 μ M) for 24 h (H). Next, the cells were
909 harvested to determine the efficiency of IRE1 α knockdown (F) or miR-30a-5p
910 expression (G, H). The results represent three independent experiments.

911 **Fig. 3. miR-30a-5p inhibits the replication of TGEV.** (A-B). The inhibition of
912 IRE1 α by 4 μ 8c suppressed TGEV infection (MOI=1) in ST cells. ST cells were
913 pretreated with 50 or 100 μ M 4 μ 8c for 2 h and then infected with TGEV
914 (MOI=1); TGEV viral RNA (A) and titers (B) were measured at 24 hpi. (C-D).
915 IRE1 α knockdown by siRNAs decreased TGEV replication. ST cells were
916 transfected with IRE1 α siRNA or siRNA scrambled control at 100 nM, followed
917 by infection with TGEV (MOI=0.01); TGEV viral RNA (C) and titers (D) were
918 quantified at 24 hpi. *, $p<0.05$, **, $p<0.01$ vs. siRNA NC. (E-G). miR-30a-5p
919 overexpression inhibited TGEV infection. ST cells were transfected with
920 miR-30a-5p mimics at the indicated doses (20, 80 and 160 nM) for 24 h,
921 followed by infection with TGEV for 24 h at a MOI of 0.01. TGEV infection was
922 determined at 24 hpi by RT-qPCR (E) or titration (F). *, $p<0.05$, ***, $p<0.001$ vs.
923 mimic NC. (G). The suppression of TGEV infection by miR-30a-5p was
924 confirmed by IFA. (H). miR-30a-5p suppressed TGEV replication at the late
925 stages of infection. ST cells were transfected with 160 nM miR-30a-5p mimics
926 for 24 h and then infected with TGEV at a MOI of 0.01. TGEV infection was
927 analyzed at 2, 6, 12, 24, or 36 hpi. (I). The miR-30a-5p inhibitor rescued TGEV
928 suppression by 4 μ 8c. ST cells were transfected with 160 nM miR-30a-5p

929 inhibitor or NC inhibitor. After 24 h of transfection, ST cells were treated with
930 100 μ M 4 μ 8c for 2 h and then infected with TGEV (MOI=1). TGEV infection
931 was measured at 24 hpi.

932 **Fig. 4. miR-30a-5p enhances IFN-I antiviral signaling rather than IFN-I**
933 **production.** (A). miR-30a-5p did not manipulate IFN- β production. ST cells

934 were transfected with 160 nM miR-30a-5p mimics or NC mimics for 24 h,
935 followed by infection with TGEV (MOI of 0.01) for 24 h. The IFN- β levels in
936 supernatant were measured by ELISA. (B-C). TGEV infection antagonized

937 interferon signaling at the late stages of infection. ST cells were infected with
938 TGEV at a MOI of 1, and then the samples were collected at different times for
939 the quantification of ISG15, IFN- β and miR-30a-5p expression (B) or the

940 Western blotting analysis of pSTAT1, STAT1 or β -actin (C). (D). TGEV infection
941 impaired IFN-I elicited STAT1 signaling. ST cells were infected with TGEV at a
942 MOI of 1 for 36 h, followed by stimulation with IFN- β for 30 min. Then, cells

943 were lysed and collected for Western blotting analysis of pSTAT1, STAT1 or
944 β -actin. (E). miR-30a-5p modulated the activity of the ISRE reporter vector
945 following IFN- β stimulation. The ISRE reporter vector and pRL-TK were

946 cotransfected with the indicated miR-30a-5p mimics, NC mimics, miR-30a-5p
947 inhibitor, or NC inhibitor into ST cells for 24 h, followed by stimulation with
948 IFN- β (100 ng/mL). Cells were harvested for luciferase assay at 12 h after

949 IFN- β stimulation. (F-H). miR-30a-5p promoted IFN- β signaling. The cells were
950 transfected with 160 nM miR-30a-5p mimics, NC mimics, miR-30a-5p inhibitor,
951 or NC inhibitor for 24 h, followed by IFN- β treatment or TGEV infection

952 (MOI=1). The samples were collected at 24 h after TGEV infection or IFN- β
953 stimulation for the quantification of ISG expression (F, G) and for Western
954 blotting analysis of pSTAT1, STAT1 or β -actin (H). Quantifications were

955 normalized to the mock-treated and uninfected NC control. (I). miR-30a-5p
956 enhanced the anti-TGEV activity of IFN- β . After transfection with miR-30a-5p
957 mimics or inhibitor for 24 h, cells were pretreated with IFN- β or DMEM for 24 h

958 and then infected with TGEV (MOI=0.01) and harvested at 24 hpi for viral RNA

959 quantification.

960 **Fig. 5. miR-30a-5p targets the 3' UTRs of SOCS1 and SOCS3.** (A).

961 Schematic diagram of the predicted target sites of miR-30a-5p in SOCS1 and
962 SOCS3 3' UTRs of six representative mammals. The predicted target sites and

963 mutated target sites of miR-30a-5p are underlined and were mutated as

964 indicated. (B). The results of the luciferase assay. ST cells were cotransfected

965 with SOCS1 or SOCS3 wild-type or mutant luciferase vectors (500 ng), and

966 160 nM miR-30a-5p mimics or NC mimics, miR-30a-5p inhibitor or NC inhibitor,

967 and the luciferase activity was analyzed at 30 h after transfection. (C). The

968 suppression of SOCS1 and SOCS3 mRNA levels by miR-30a-5p under

969 TGEV-uninfected conditions. ST cells were transfected with 160 nM NC

970 mimics, miR-30a-5p mimics, NC inhibitor, or miR-30a-5p inhibitor. The

971 expression levels of SOCS1 and SOCS3 were analyzed by RT-qPCR at 48 h

972 after transfection. The relative expression of SOCS1 and SOCS3 was

973 normalized to that of the NC control. Bars represent the means \pm SEM (n=3).

974 (D). The suppression of SOCS1 and SOCS3 protein levels by miR-30a-5p

975 under TGEV-uninfected and infected conditions. ST cells were transfected as

976 described in panel C for 24 h, followed by infection with TGEV (MOI=1) or

977 mock DMEM, and the samples were collected at 24 h for Western blotting

978 analysis of SOCS1, SOCS3 or β -actin. Quantifications were normalized to the

979 uninfected NC control. (E-G) TGEV infection upregulated SOCS1 and SOCS3

980 expression. The SOCS1 and SOCS3 expression levels (E) in ST cells were

981 measured by RT-qPCR at 24 hpi with different MOIs. *p* represents the

982 difference vs. the mock-infected control. For time kinetics, the SOCS1 and

983 SOCS3 mRNA levels (F) or SOCS1 and SOCS3 protein levels (G) in ST cells

984 were measured at indicated time points after infection with TGEV at a MOI of 1.

985 (H). Treatment with 4 μ 8c abolished the upregulation of SOCS1 and SOCS3 by

986 TGEV infection via modulating miR-30a-5p. ST cells were transfected with 160

987 nM miR-30a-5p inhibitor for 24 h. Next, ST cells were pretreated with 100 μ M

988 4 μ 8c or DMSO for 2 h followed by infection with TGEV (MOI=1). Cells were

989 collected for RT-qPCR analysis for SOCS1 and SOCS3 expression at 24 hpi.
990 (I-J) Elevated expression of SOCS1 and SOCS3 in the ilea after TGEV
991 infection. The expression of SOCS1 (I) and SOCS3 (J) in the ilea at 48 hpi was
992 quantified by RT-qPCR. Bars represent the means \pm SEM.

993 **Fig. 6. Increased expression of SOCS1 or SOCS3 dampens the IFN-I**
994 **antiviral response and promotes TGEV replication.** (A). Overexpression of
995 SOCS1 and SOCS3 in ST cells. ST cells were transfected as indicated with
996 pCAGGS-HA, pCAGGS-SOCS1 or pCAGGS-SOCS3 for 48 h, and the
997 transient expression of SOCS1 and SOCS3 was confirmed by IFA with anti-HA
998 staining. (B). SOCS1 or SOCS3 overexpression suppressed the activation of
999 STAT1 by IFN- β and TGEV infection. ST cells were transfected as indicated
1000 with pCAGGS-HA, pCAGGS-SOCS1, or pCAGGS-SOCS3 for 24 h, followed
1001 by incubation with porcine IFN- β (100 ng/mL) or infection with TGEV (MOI=1).
1002 Cells were collected for Western blotting analysis of pSTAT1, STAT1 or β -actin
1003 after 24 h. *p* represents the difference vs. the vector control. (C-D). SOCS1 or
1004 SOCS3 overexpression enhanced TGEV infection and undermined the
1005 anti-TGEV activity of IFN- β . ST cells were transfected as described in panel B,
1006 followed by incubation with porcine IFN- β (C) or DMEM (D) for 24 h. Then,
1007 cells were infected with TGEV at a MOI of 0.01; TGEV infection was
1008 determined at 24 hpi. (E). Knockdown of SOCS1 and SOCS3 by siRNAs in ST
1009 cells. ST cells were harvested for Western blotting analysis of SOCS1 and
1010 SOCS3 expression at 48 h after transfection with 100 nM siSOCS1s,
1011 siSOCS3s, or scrambled control siRNA. (F). Enhancement of anti-TGEV
1012 activity of IFN- β by knockdown of SOCS1 or SOCS3 in ST. ST cells were
1013 transfected with siSOCS1s, siSOCS3s, or the scrambled control for 24 h,
1014 followed by incubation with IFN- β for 24 h. Then, cells were infected with
1015 TGEV (MOI=0.01) and harvested for quantification of TGEV infection at 24 hpi.
1016 (G) Silencing of SOCS1 or SOCS3 boosted IFN- β signaling under
1017 IFN- β -stimulated conditions. ST cells were stimulated with IFN- β at 24 h after
1018 transfection with siSOCS1#1, siSOCS3#3, or the scrambled control, and cells

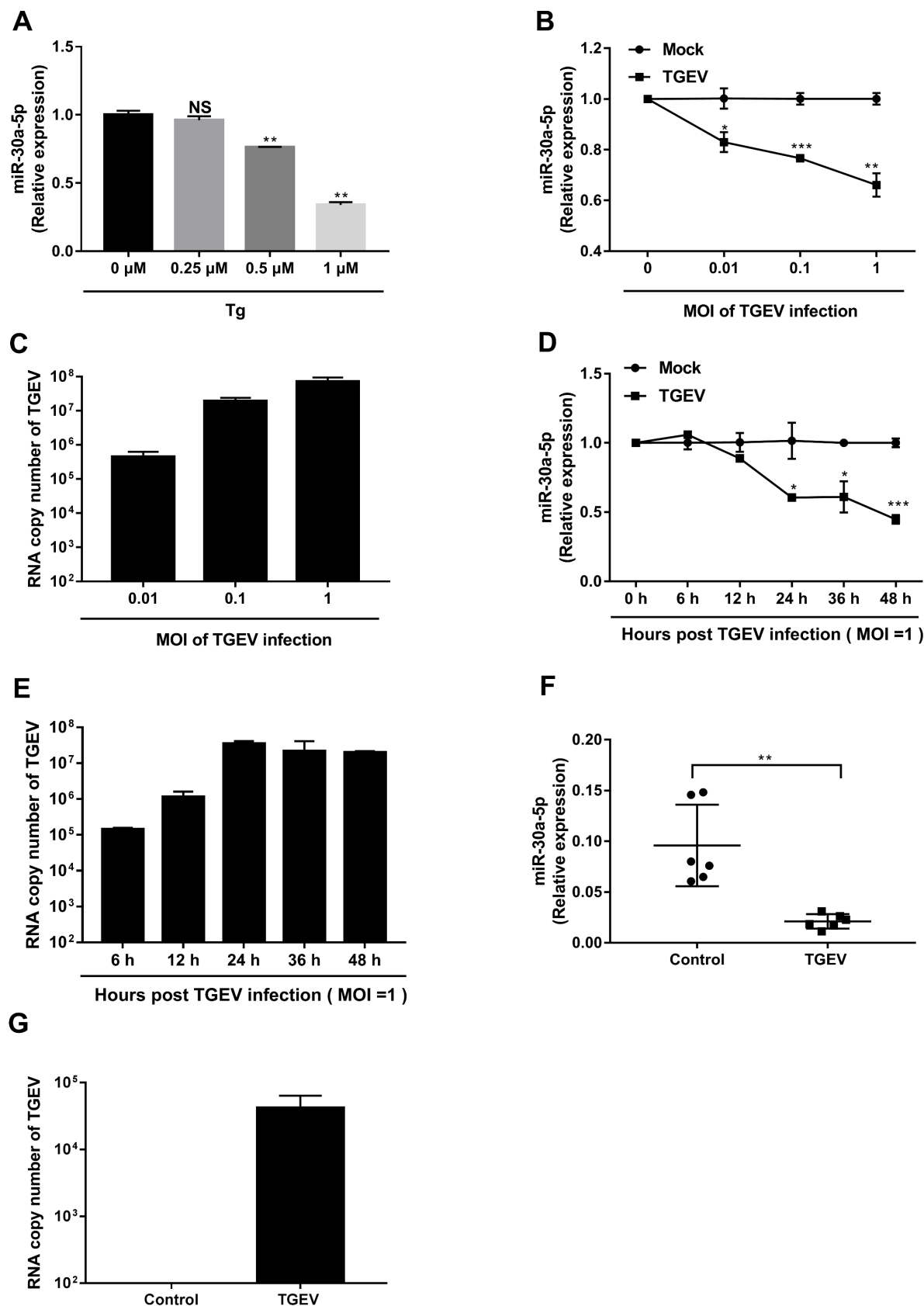
1019 were collected for RT-qPCR analysis of ISG15, OASL, or MxA expression
1020 relative to that of GAPDH after 24 h stimulation. (H) Silencing of SOCS1 or
1021 SOCS3 decreased TGEV infection under IFN- β unstimulated conditions. ST
1022 cells were transfected with siSOCS1#1, siSOCS3#3, or the scrambled control
1023 for 24 h. Then, cells were infected TGEV (MOI=0.01) and harvested for
1024 quantification of TGEV infection at 24 hpi. (I) Silencing of SOCS1 or SOCS3
1025 boosted IFN- β signaling under TGEV-infected conditions. ST cells were
1026 treated as described in Panel H, and cells were collected for RT-qPCR
1027 analysis of ISG15, OASL, or MxA expression relative to that of GAPDH.

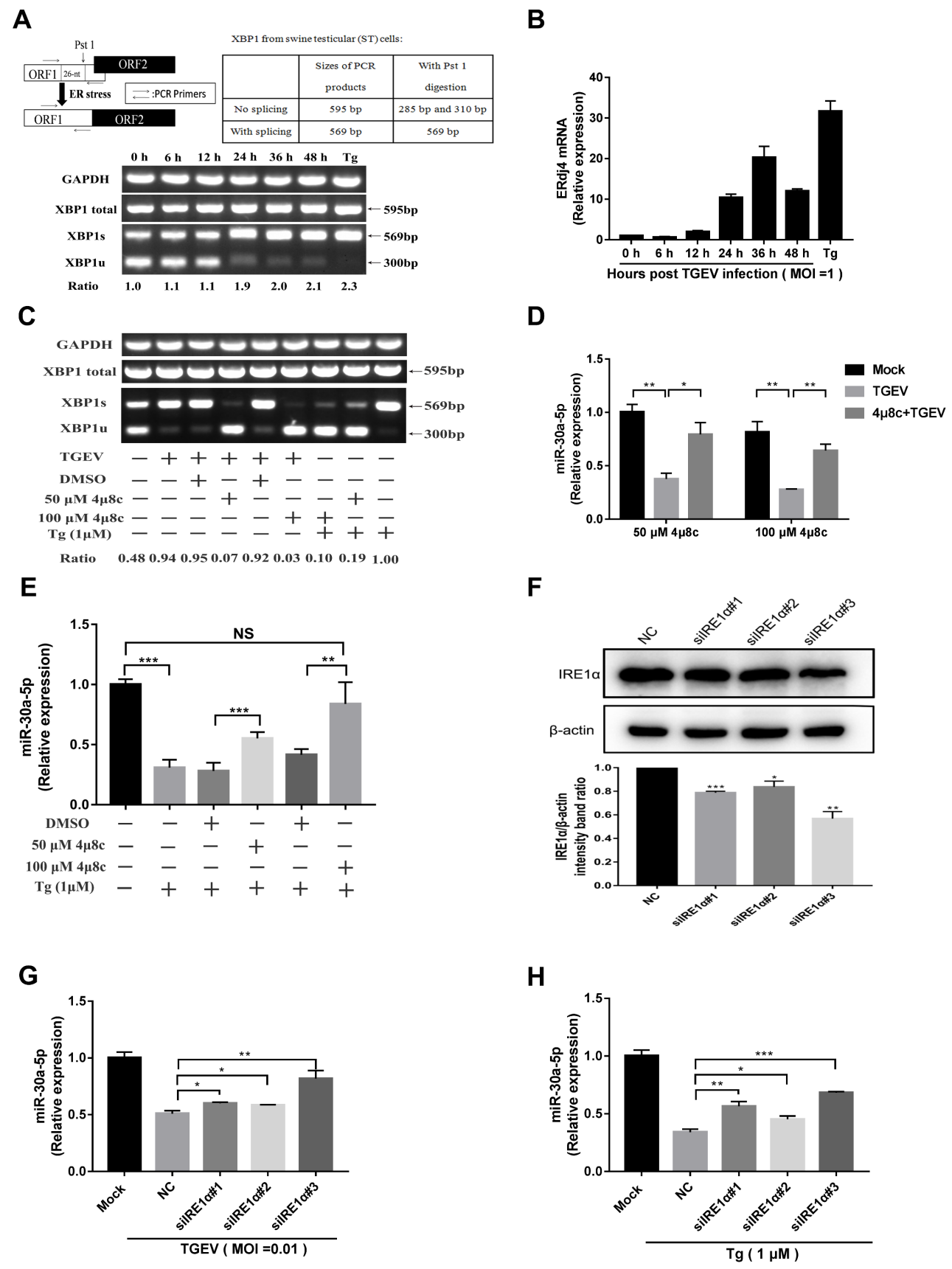
1028 **Fig. 7. IRE1 α facilitates TGEV infection by modulating the**
1029 **miR-30a-5p/SOCS axis**

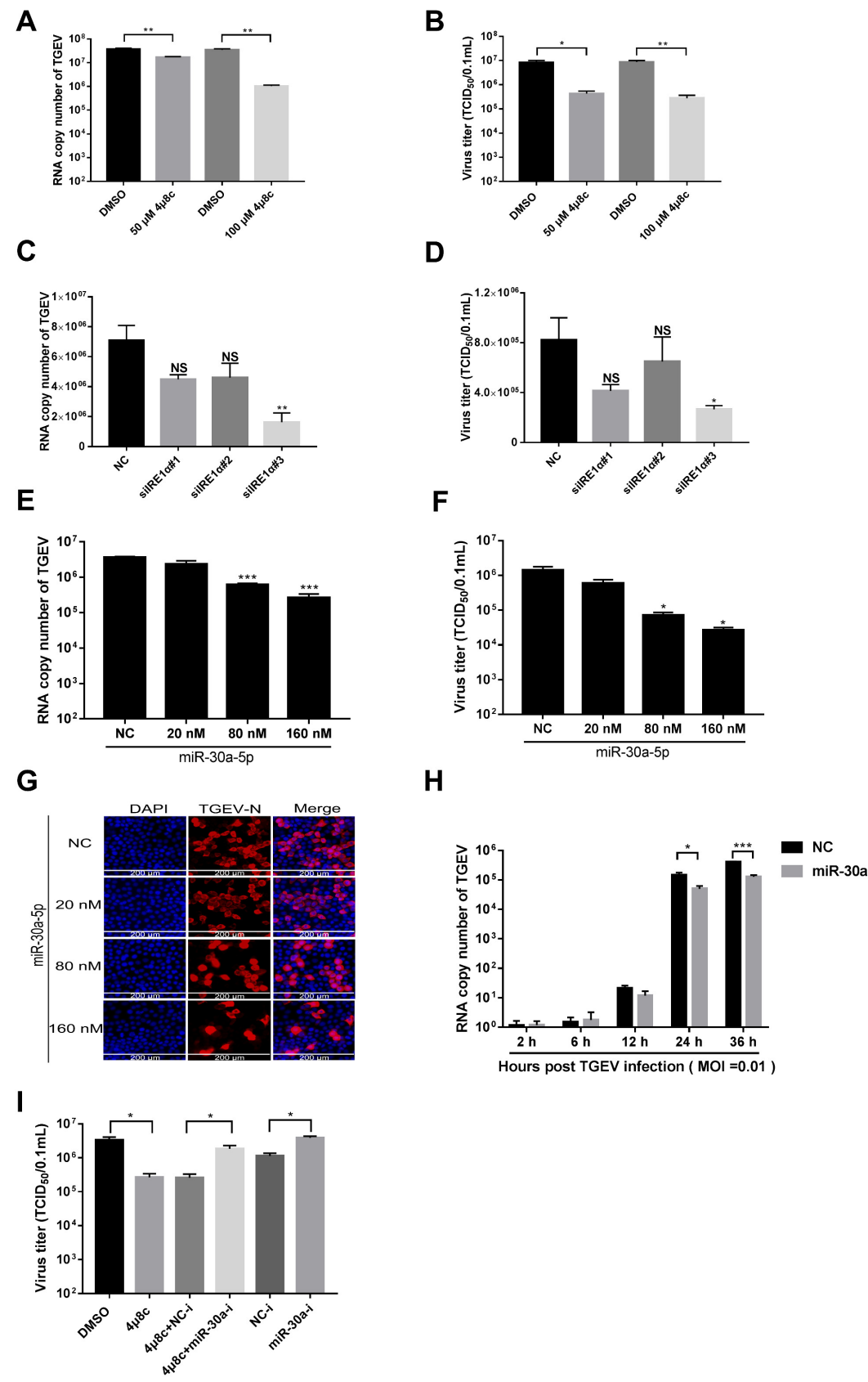
1030 (A-B) The blockage of STAT1 activation rescued the viral suppression of 4 μ 8c.
1031 ST cells were pretreated with 100 μ M 4 μ 8c for 2 h or 100 μ M 4 μ 8c for 2 h plus
1032 10 μ M fludarabine for 24 h, followed by infection with TGEV (MOI=1). Then,
1033 the TGEV titer (A) was measured at 24 hpi, and STAT1 and p-STAT1 were
1034 analyzed by Western blotting (B). (C-D). The blockage of STAT1 activation
1035 rescued the viral suppression of miR-30a-5p. ST cells were transfected with
1036 160 nM NC mimics, miR-30a-5p mimics or miR-30a-5p mimics plus 10 μ M
1037 fludarabine stimulation for 24 h, followed by infection with TGEV (MOI=1). Next,
1038 the TGEV titer (C) was measured at 24 hpi, and STAT1 and p-STAT1 were
1039 analyzed by Western blotting (D). (E) Effect of 4 μ 8c and fludarabine on cell
1040 viability. ST cells were treated with 4 μ 8c, 4 μ 8c plus fludarabine, fludarabine
1041 only, or the carrier control DMSO as described above. Cell cytotoxicity was
1042 analyzed with a CCK-8 system as described in the Materials and Methods. (F)
1043 Knockdown of IFNAR1 by siRNAs in ST cells. ST cells were harvested for
1044 RT-qPCR analysis of IFNAR1 expression at 48 h after transfection with 100 nM
1045 siRNAs or scrambled control siRNA. (G) Silencing of IFNAR1 dampened IFN- β
1046 signaling under IFN- β -stimulated conditions. ST cells were transfected with
1047 100 nM siIFNAR1#1 or scrambled control siRNA for 24 h, followed by
1048 incubation with IFN- β for 24 h. Then, cells were collected for RT-qPCR

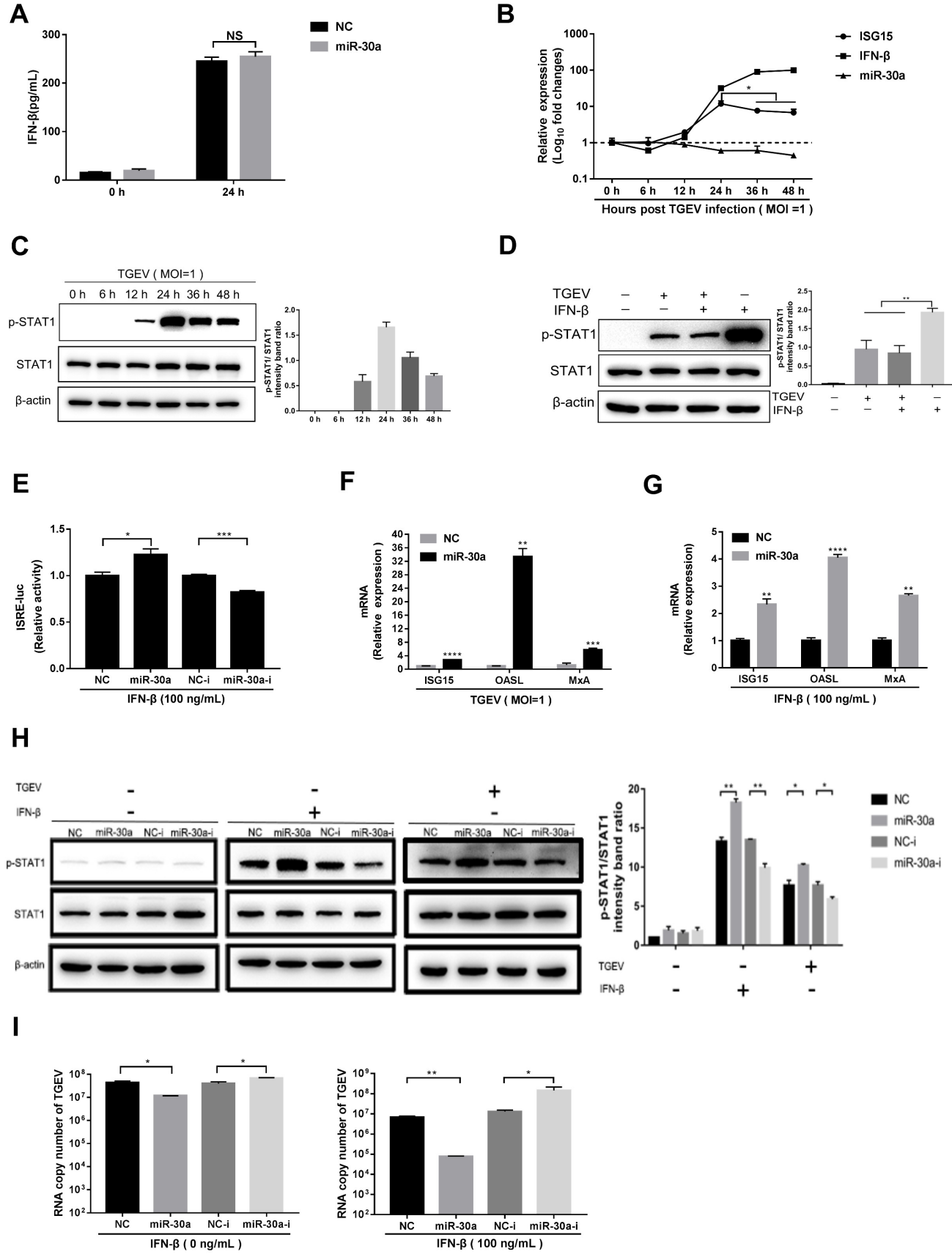
1049 analysis of ISG15, OASL, or MxA expression relative to that of GAPDH. (H and
1050 I). Silencing of IFNAR1 abolished the viral suppression (H) and enhancement
1051 of p-STAT1 (I) of miR-30a-5p. NC mimics or miR-30a-5p mimics (160 nM)
1052 were cotransfected with 100 nM siIFNAR1#1 or the scrambled control in ST
1053 cells for 24 h, followed by infection with TGEV (MOI=1). The TGEV titer (H),
1054 STAT1 and p-STAT1 (I) were measured at 24 hpi.

1055 **Fig. 8. TGEV antagonizes IFN-I-related innate immunity via**
1056 **IRE1 α -mediated manipulation of the miR-30a-5p-SOCS axis.** During TGEV
1057 infection, TGEV activates IRE1 α , which reduces miR-30a-5p abundance. The
1058 decreased level of miR-30a-5p dampens IFN-I antiviral signaling by increasing
1059 the expression of SOCS1 and SOCS3, leading to viral escape from the IFN-I
1060 response.

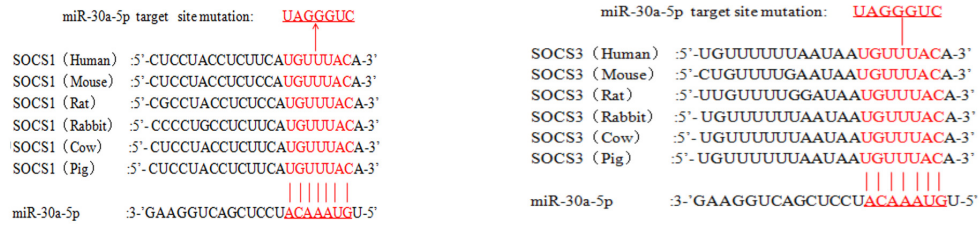




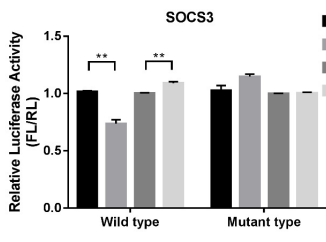
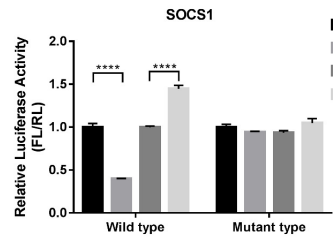




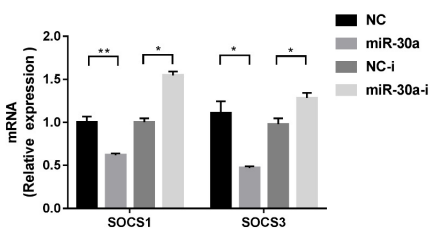
A



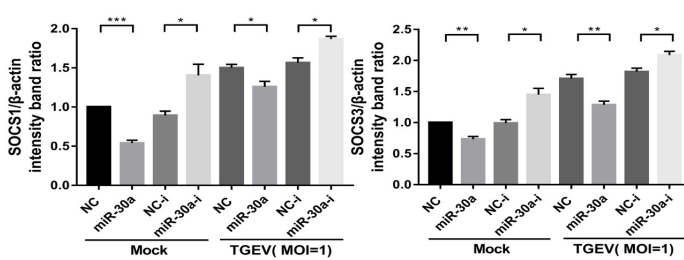
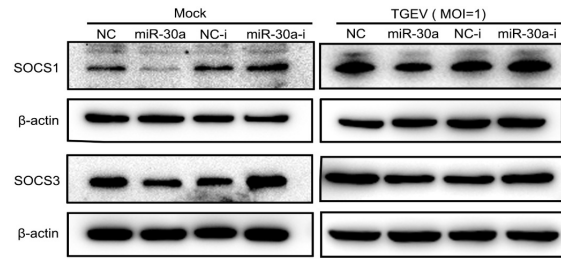
B



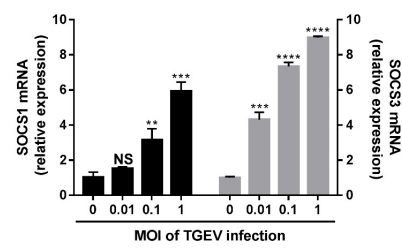
C



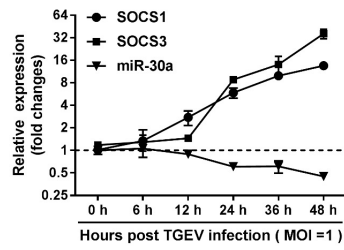
D



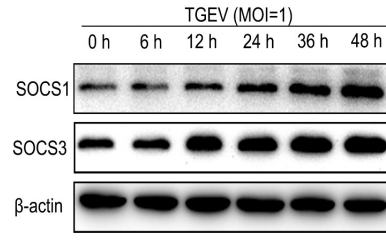
E



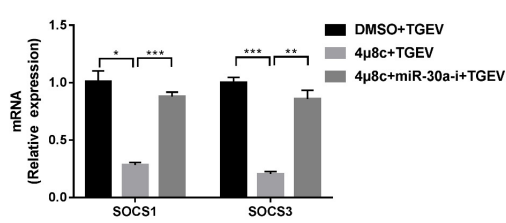
F



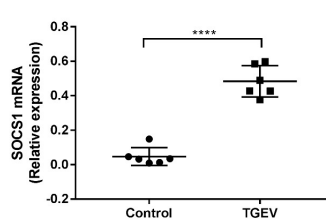
G



H



I



J

